SINTERING BEHAVIOR OF PREALLOYED BRONZE THROUGH SUPERSOLIDUS LIQUID PHASE SINTERING

By

Pampa Ghosh

DEPARTMENT OF MATERIALS AND METALLURGICAL ENGINEERING

Indian Institute of Technology Kanpur

JUNE, 2003

SINTERING BEHAVIOR OF PREALLOYED BRONZE THROUGH SUPERSOLIDUS LIQUID PHASE SINTERING

A Thesis Submitted

In Partial Fulfillment of the Requirements

For the degree of

Master of Technology

by

Pampa Ghosh

(Roll No. Y120612)

to the

DEPARTMENT OF MATERIALS AND METALLURGICAL ENGINEERING

INDIAN INSTITUTE OF TECHNOLOGY KANPUR

JUNE, 2003

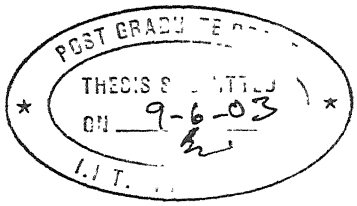

CERTIFICATE

This is to certify that the work contained in the thesis entitled **"Sintering Behavior of Prealloyed Bronze through Supersolidus Liquid Phase Sintering"** by Pampa Ghosh (Roll No. Y120612) has been carried out under our supervision and to the best of our knowledge this work has not been submitted elsewhere for a degree.

Dr. R. K. Ray
Professor
Department of Materials and
Metallurgical Engineering
Indian Institute of Technology,
Kanpur

Dr. Anish Upadhyaya
Assistant Professor
Department of Materials and
Metallurgical Engineering
Indian Institute of Technology,
Kanpur

To...

My Dear Sister

Acknowledgements

I would like to express my gratitude to my thesis supervisors Prof. R.K. Ray and Dr. A. Upadhyaya for their guidance during my post graduate study at Indian Institute of Technology, Kanpur.

I want to specially thank Mr. V. Kumar and Mr. U. S. Singh for their untiring support at various stages of this work.

I also acknowledge the help provided by Dr. Mungole and Mr.S.C.Soni during the experimental work.

This occasion is perfectly befitting to acknowledge the help and support provided by Anirban, Chiradeep, Kausik, Pinakida, and Rajibda. My association with them will be ever-cherishable memory in my life. I also sincerely remember and acknowledge 'Kakima' (Mrs Ray), and also Rupa; providing me moral supports during the hard time I faced in IIT, Kanpur.

This is the right occasion to remember with reverence the supports provided by my family. I could not have come this far without their unconditional love and encouragement.

Pampa Ghosh.

Contents

ABSTRACT

The sintering behaviour of Cu-12% Sn prealloyed bronze powder has been investigated in the present work The research is mainly focused on the supersolidus liquid phase sintering technique applicable to this system in order to achieve certain properties, which haven't been obtained so far by conventional technique. The main use of bronze is limited to the fabrication of porous or self-lubricating bearing. The present work has been carried out to look into the possibility of using bronze in structural applications. For the purpose of attaining good corrosion resistance property, prealloyed bronze powders have been used. Two different pressure conditions have been chosen for compaction. The main aim has been to determine the effect of pressure and sintering temperature on the properties of the sintered component Supersolidus Liquid Phase Sintering has been performed at four different temperatures depending upon the liquid formation, which can be determined from the phase diagram The results obtained on the supersolidus sintered samples have been compared with those of solid state sintered samples.

The characterization of the sintered products; such as density, densification parameters, porosity, and hardness have been carried out. Macrographs and microstructures of all the sintered samples have also been captured. In addition, attempt has been made to determine the effect of pressure and sintering temperature on the evolution of phases of the compacts using XRD.

List of Figures

List of Tables

Chapter 1...

INTRODUCTION

INTRODUCTION

Bronze was widely used for utilitarian and artistic purposes until iron became cheaper and more plentiful. Bronze continued to have wide utilitarian uses until it became cost prohibitive. Now other than applications such as a bearing metal in the engineering and automobile industries, bronze is also used in structural parts, preferably where good corrosion resistance is necessary. Artistically, bronze is still widely used in casting sculptures of all sizes, plaques, and bells.

Bronze still constitutes a significant tonnage use for tin and is likely to remain so in the foreseeable future. Many different copper alloys exist, some of which constitute alternative materials to tin bronze, but for many specific applications (self lubricating bearing, filters etc.) tin bronzes are still indispensable. Gunmetals are bronzes which contain additionally some zinc and these are widely used as casting alloys in place of binary bronzes.

Bronzes are utilized in three forms – as castings, as wrought material and as sintered powder components for special applications

- *Wrought bronzes:* These contain tin up to 8%.
- *Cast bronzes:* These bronzes have Sn from 8 to 20%.
- *Sintered bronze:* These bronzes have tin from 5 to 15%.

Sintering of powder compacts allows fabrication of near net shape components with densities approaching theoretical values. Liquid phase sintering (LPS) involves the presence of liquid phase at the sintering temperature, in addition to the solid phase. Generally, an additive powder either melts or reacts to form a liquid phase between the particles resulting in rapid densification. Liquid phase sintering is very effective in reducing the sintering temperature and enhancing the densification of coarse powders where solid state sintering does not give significant densification.

However, there is another approach of LPS, where liquid will form from the alloy itself; i.e.; sintering temperature is kept between solidus and liquidus lines. This is called super-solidus liquid phase sintering (SLPS). Including the common advantages of LPS, SLPS also has other advantages also. The distribution of liquid is far better than that of ordinary LPS as here liquid is generated at the grain boundaries. Thus SLPS is an

attractive approach for processing prealloyed powders and was not much used in the powder metallurgy industry because of associated problems. A practical difficulty lies in process control, especially with respect to the acceptable temperature range for sintering. In many alloy systems, a temperature window is extremely narrow (10-20°C above the solidus). In addition, the interaction between process parameter such as heating rate and sintering time, and material parameters such as powder chemistry, particle size, and grain size are important.

This thesis focuses on the sintering of prealloyed bronze powders having a composition of Cu-12%Sn. Chapter 2 gives the background for the study. This includes phase diagrams of bronze and the development of powder metallurgy (P/M) bronze, and a review over super-solidus liquid phase sintering, in general.

In Chapter 3 scope of the present work is discussed. Chapter 4 describes in detail the experimental procedure. It includes the methodology for powder characterization, and compaction process. In addition, the sintering procedure is also discussed in detail. This is followed by a brief description about the xylene impregnation, XRD studies and metallographic procedures. Chapter 5 deals with the experimental results. Chapter 6 and 7 consist of discussion and conclusions, respectively.

Chapter 2...

BACKGROUND

BACKGROUND

2.1 Bronze

Copper was the first metal known to man and has lost none of its fascination to this day. The history of copper stretches back to the Stone Age when it was first discovered by man in its native stage and fashioned into the first metal objects. Since then copper has been an indispensable part of our cultural history and industrialization. It was first smelted around 4500 BC and extraction of ores started around 3900 BC. In the year 3500 BC, tin bronzes first appeared as the oldest alloy in the history of mankind. Bronzes, being the oldest utility alloy and have given their name to a whole era of human history – The Bronze Age. The first bronze artifacts were produced in Egypt around 2800 BC. Many Roman and Greek coins were made from tin bronze [1].

Generally, all copper-tin alloys with more than 78% copper are called bronzes. The use of tin bronze has remained economically viable in part due to the recycling of scrap. The attractive and useful properties of copper tin alloys, combining moderate strength, corrosion resistance and very good cold working properties, makes them one of the most important metals. Since these alloys frequently display an adequate electrical and thermal conductivity and are highly suitable for brazing and soft soldering, they are used for heavily stressed contact spring in the field of electronics and electrical engineering area for plug connectors. They are chemically very stable. When in dry air the metal does not get oxidized, while in moist air it produces a beautiful, green, pore-free, surface film (patina) which protects the layers it covers from corrosion [2].

Bronzes are utilized in three forms – as castings, as wrought material and as sintered powder components for special applications. In general, the cast alloys may contain up to about 12% tin but there is a demand for higher tin levels (for example 15%) and for applications, such as bells and musical cymbals, 20 to 25% tin is needed to produce the required tonal qualities. Gunmetals are a cheaper substitute for certain castings, while lead to the extent of as much as 20% may be present where superior bearings properties are necessary. Industrial alloys have a maximum of 20% tin. As stated earlier the bronzes can be classified into three major groups:

Wrought bronzes: These contain up to 8% tin. These are single-phase α solid solution-bronzes having good ductility and malleability, and, thus, can be easily cold worked by rolling to sheets, bars, or by drawing to wires (for springs), and mint coins.

Cast bronzes: These bronzes have Sn varying from 8 to 20%, and can be produced only in the cast-form as these have two phase structures, $\alpha + (\alpha + \delta)$, and thus cannot be easily cold worked. These bronzes may have larger content of zinc and phosphorous. These have high corrosion resistance, low shrinkage and high antifriction properties. These bronzes can be divided into three classes

Cast bronzes having 8 to 12% tin: These are used for casting pumps, gears, machine parts, heavily loaded bearings, and marine parts to resist sea-water corrosion Cast bronzes having 12 to 20% tin: These are mainly used for bearings. Bronzes having 20 to 25% tin: Bell metals are used for making bells. They are very hard and relatively brittle. They can only be cast

Sintered bronze: Powder metallurgy bronzes typically originate as premixes consisting of elemental copper plus 0 5 to 0.75% dry organic lubricants such as stearic acid or zinc stearate. These bronzes have tin from 5 to 15%. Some of structural parts,

however, are fabricated from prealloyed powder. A wide range of bronzes and leaded bronzes is manufactured by the powder metallurgy route, usually by atomization of prealloyed metal but sometimes by sintering together elemental powders.

2.2 Copper-Tin Phase Diagram

The binary copper-tin equilibrium diagram is given in Figure 2.1 [3]. This figure shows the truncated version of equilibrium diagram contains up to 35 wt. % Sn. This much amount of Sn is mainly used for industrial purpose. However the full version of copper-tin equilibrium is shown in Figure 2 2 Copper-tin phase diagram consists of several peritectic reactions, and two eutectoid reactions. The solid solubility of tin in copper decreases from 11% at 350°C to around 1% at room temperature. At 520°C, γ-phase undergoes eutectoid reaction to form a mixture of (α +δ)-phases. Then, δ decompose to produce a mixture of (α +ε)-phases by eutectoid reaction at 350°C. The reactions occurring at lower temperatures are very low in nature and, equilibrium is not easily attained even at 600°C. In commercial bronzes, the phase ε phase is normally non-existent, and cast alloys have a structure of α + (α +δ) eutectoid. The δ-phase, based on electron compound $Cu_{31}Sn_8$, is pale-blue in color, hard and brittle [3]. This decreases the strength and elongation. However, alloys up to 8% tin usually show single phase, α solid solution at room temperature. Whereas, bronzes with higher than 8% tin are neither rolled nor forged as δ makes them brittle, and are used only for castings.

From the practical view-point α and δ phases are the only ones likely to be present at room temperature in most commercial bronzes. It will be better if the hard δ phase is distributed uniformly in the soft α matrix.

The body centered cubic structures β and γ are metastable phases which transform on slow cooling; they can be retained to some extent by quenching, more especially if the tin content of the alloy exceeds about 20%. These phases are ductile which is of practical importance in connection with the hot working of bronzes The ζ and η phases have hexagonal structures, corresponding to $Cu_{20}Sn_6$ and Cu_6Sn_5 respectively, the latter being regarded as a superlattice based on nickel arsenide structure. These phases are unlikely to be found in commercially produced bronzes although sometimes η may be formed by diffusion reaction. The ε phase has an orthorhombic structure and corresponds to the composition Cu_3Sn [4].

Changes in the solid solubility of tin in copper below 500°C proceed so sluggishly that as far as the normal production, heat treatment and fabrication of bronze are concerned it is permissible to modify the equilibrium diagram to show the δ phase existing down to the room temperature and the α phase boundary as a vertical line at 16% tin exceeding from just below 600°C to room temperature. Annealing at or above 500°C followed by slow cooling retains 13% to 16% of tin in solid solution, the exact amount retained being dependent on the time and temperature.

The addition of tin increases the strength significantly as well as ductility of copper but steep drop in ductility takes place around 8% tin The strength falls drastically at 25% Sn, when the structure contains too much brittle δ phase. Thus, tin content above 25% is less important for industrial applications, rather they are only for academic interest. The presence of hard eutectoid in the cast structure ensures a high resistance to wear and abrasion 10% Sn alloy is best antifriction material, and is widely used as a ball-bearing alloy [4]

Cast tin-bronzes invariably show pronounced coring as there is a wide separation of the liquidus and solidus curves, and the diffusion takes place very slowly By powder metallurgy route we can avoid the coring by proper selection of sintering temperature and time.

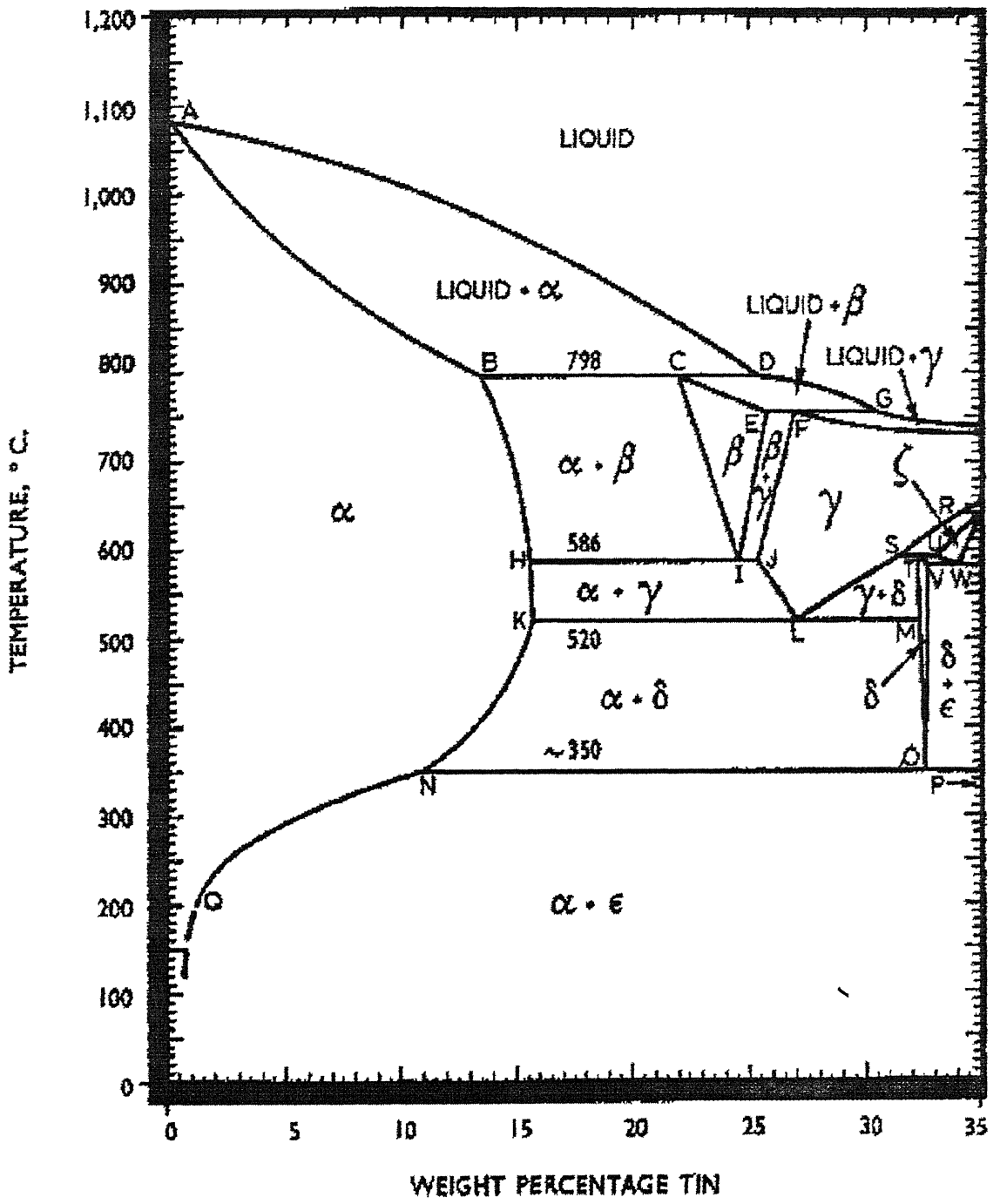

Figure 2.1 Copper-Tin Equilibrium Diagram [3].

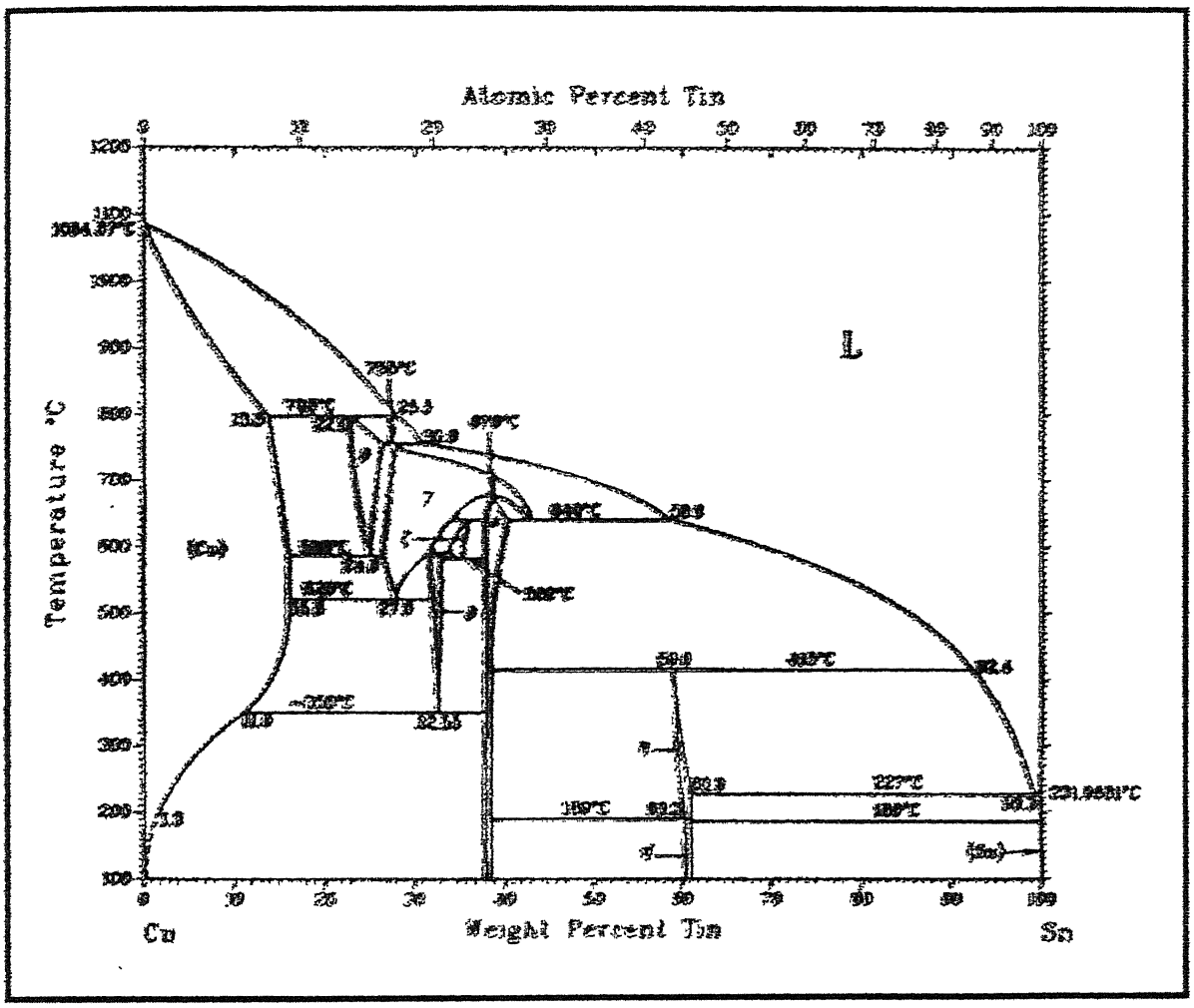

Figure 2.2 Copper-Tin Equilibrium Diagram [4].

2.3 P/M Bronze

The methods of ancient powder metallurgy offered the possibility of making tools and weapons from iron and its alloys, and this marked the transition of humanity from barbarism to the civilized state [5]. Advancement in electrical engineering, the electric lamp industry and electronics, the metal working industry, etc at the end of the nineteenth century and in the first half of the twentieth century, led to the emergence of powder metallurgy as a means of production of refractory metals and chemical compounds, in particular hard alloys. The role of powder metallurgy is quite clearly apparent in solution of prospective problems of the future; efficient synthesis of materials with pre-specified properties [6].

Copper base powder metallurgy products rank third after iron and steel, and aluminum base P/M product in terms of volume. The estimated shipments of copper and copper base alloy powder in 1996 were about 23,000 tons in North America. The shipments in Europe were estimated to be about 15,600 tons while the shipments in Japan were estimated about 7,000 tons [7].

Among copper base P/M alloy bronze is the most extensively used. P/M bronzes typically originate as premixes consisting of elemental copper and tin powders plus 0.5 to 0.75 % dry organic lubricants such as stearic acid or zinc stearate. These lubricants can be mixed with the powders before pressing (i.e. admixed) or can be used as the die wall lubricant during pressing. This is necessary to reduce friction between the powder and the tooling surfaces (die cavity, punches, and core rods), permitting higher effective pressures to be transmitted to the powder mass and thus yielding a higher compacted (green) density for a given applied pressure. Some structural parts, however, requiring densities greater than 7.0 g/cm^3 are fabricated

from prealloyed powders; whereas the theoretical density for 90Cu-10Sn is around 8.77 g/cm^3. Premixed and the prealloyed powders have been in use depending on the applications of P/M bronze. Due to solid solution strengthening, prealloyed powders have higher yield strengths and work hardening rates than premixed powders. Generally atomization technique is preferred for the production of copper, tin or the prealloyed powders. Spherical powders are preferred for producing porous bronze. Gas atomization technique is the most popular technique in this respect. Water atomized powders are irregular in shape because of the comparatively high cooling rate than in the gas atomization technique For spherical samples the contact area between the particles is less, so the chance of bonding and therefore green strength is also low. But as these bronze products are generally used as porous body where the strength is not the main criteria, spherical powders are quite useful. For structural application strength is important and therefore irregular water atomized powder is to be preferred. Pressing loads required to achieve given green densities in prealloyed powders are higher than the pressures required for elemental powder mixes. Depending on applications, sintering furnace temperatures for bronze range from 350 to 870°C; total sintering time within the hot zone may range from 15 to 30 min, depending on the furnace temperature selected [8]. It also depends upon the required dimensional change and most importantly, the presence of an optimal α-bronze in the matrix. Sintering atmospheres should be protective, preferably reducing to aid densification during sintering. Generally, reducing atmosphere is used during sintering, such as, nitrogen, hydrogen or cracked ammonia to reduce the chance of oxidation of powders. The reduction of the surface oxides of copper and tin leads to an increased diffusion rates.

It is found that the copper-tin blends of coarser powder have shown the higher growth values than a blend composed of finer powders The final dimensional change during the sintering procedure depends a lot on the powder characteristics (i.e shape, size, morphology) So the proper choice of the powders plays a very important role in terms of getting the desired product. Sintering is favored by the decrease in the interfacial energy and typically leads to shrinkage due to the elimination of pores when sintering takes place at elevated temperatures, the rate of mass transport is increased and this enhances diffusion. Consequently the point contacts between the contacting particles form interparticle necks, which cause dimensional changes. However in case of bronze tin melts and goes into the copper matrix due to its high solubility in copper. This leads to the expansion of the lattice and tin sites leave behind the pores in the microstructure. This phenomenon is called bronze compact growth.

Properties of P/M Bronze

P/M bronze has good mechanical strength and hardness which are quite comparable with the cast product Comparison of different mechanical properties of cast, wrought and P/M bronze are summarized in Table 2.1. Typically, P/M bronze inherently has residual porosity. This leads to decrease in the electrical and thermal conductivity. Bronze produced by P/M route shows reasonable working properties. Although porous, P/M bronze still has very good corrosion resistance properties. It shows neutral behaviour in almost all kind of environment. P/M bronze is featured by the presence of well distributed porosities throughout the matrix. These pores are subsequently infiltrated by oil, which produce excellent bearing characteristics. Bronze can be easily soldered to other alloys also.

Table 2.1 Typical properties of 90Cu-10Sn bronze processed by different route [9]

Property	Tensile Strength (MPa)	Yield Strength (MPa)	Elongation (%)	Hardness (HRB)
Wrought	420-455	180-195	30-60	97-100
Sand Cast	300-325	150-160	15-20	80-85
P/M	130-150	80-90	10-20	-

Applications of P/M Bronze

The use of P/M Bronze dates back to the 1920s, when commercially porous bronze bearings were developed independently in the research laboratories of General Motor Corporation [10,11] and Bound-Brook Oilless Bearing Company [12] These self lubricating bearings still account for the major portion of P/M Bronze applications. Other important applications are summarized in Table 2.2 include friction materials, brushes, filters, electrical parts, catalyst, paints, pigments, and structural parts. Other recent trends of bronze applications are in the area of automotive and industrial equipments

Table 2.2 Applications of P/M Bronze [9]

Applications	Equipments
Self Lubricating Bearings;	
i Home Appliances	Dish washers, clothes driers, washing machine, sewing machine, vacuum cleaners, refrigerators, food mixers.
ii. Farm and lawn	Tractors, combines, cotton tickers, lawn mowers, string cutters, chain saws.
iii Consumer electronics	Phonographs, record changers, tape recorders.
iv. Business machines	Type writer, computers, and copiers.
v. Industrial equipments	Textile machines, packaging machines, electric fans, portable power tools, drills, saws.
Automotive	Starters, light generators, oil and water pumps, wind shield wipers, hood and window raisers, heaters, air conditioners, power antennae, power seat adjusters, bushings.
Chemical and industrial	Filters, flame arresters.
Coatings and paints	Decorative paints, lacquers.
Construction hardware	Decorative plastics, locks and keys.
Structural parts	Paints, spraying equipments, out boat motors, automobile clutches.
Other uses	Telephone components, photographic equipments, brazing compounds.

Bearings:

Self lubricating porous bronze bearings are made by pressing elemental powder blends of copper and tin, followed by sintering The most widely used bearing material is 10% tin bronzes, often with the addition of up to 1.5% graphite. When the tin content is diminished, it is substituted by other elements (Mn, Zn, Fe etc.). This is called dilute bronze bearings. The reason for this is the high cost of tin which is the main disadvantage of these bronzes. Decreased tin content reduces the cost of this bearing at the expense of some loss in the performance [9,13].

Filters

The ability to achieve close control of porosity and pore size is the main reason filters are made from metal powders. Tin bronze is the most widely used filter materials, but Ni-Ag, stainless steel, Cu-Sn-Ni alloys, and Ni-based alloys are also used. The major advantage of P/M bronze filter materials over other porous metals is the cost. Porous P/M bronze filters have tensile strength ranging from 20-140 MPa and appreciable ductility, up to 20% elongation P/M bronze also have the same corrosion resistance as cast bronze and thus can be used in a wide range of environments. Bronze filters are usually made by sintering of spherical bronze powders, which are generally made by atomization of molten pre-alloyed bronze. These powders typically contain 90-92% copper and 8-10% tin. Deoxidizing the melt as well as alloying it with phosphors is normally done with phosphor copper such as V-CuP-10. Phosphorus increases the strength of tin bronze promoting a uniform and fine grained texture in alloy [14]. Filters made from atomized bronze have sintered densities ranging from 5.0-5.2 g/cm^3. To produce filters with the highest permeability for a given maximum pore size, powder particle of uniform particle size must be used.

Such filters are commonly used to filter gasses, oils, refrigerants, and chemical solutions.

Structural parts:

P/M bronze parts for structural applications frequently are selected because of corrosion and wear resistance of bronze. Prealloyed powders are generally used for this purpose. The powders are generally produced by atomization. In general, physical and mechanical properties of near full density Cu-Sn alloys P/M structural parts are comparable to cast and wrought Cu base material of similar composition. However, P/M Cu parts vary in density from low density typical of self lubricating bearings or filters to the near full density of electrical parts. Until now prealloyed bronze powders are not used widely for structural parts fabrication because their nodular particle forms and high apparent density results in low green density. The low end of the range for green density represents parts of complex configuration or long parts requiring deep fill. However, prealloyed powders undergo significant shrinkage during sintering with related densification of the compacts. The actual increase in density could be about 0.3 to 0.4 g/cc. Consequently it is often desirable to press at relatively low green densities and allow the part to achieve the required density through densification during sintering [15]. However, blends of such powders with irregular Cu powders and P-Cu yield sintered part with good mechanical properties.

2.4 Sintering

Sintering may be considered as the process by which an assembly of particles, compacted under pressure or simply confined in a container, chemically bond themselves into a coherent body under the influence of an elevated temperature The temperature is usually below the melting of the major constituent [16].

Sintering process can broadly be divided into two groups- solid state sintering and liquid phase sintering. Figure 2 3 shows various sintering processes and subdivisions in terms of the key processing parameters [17]. In case of solid state sintering, the sintering process is carried out at a temperature where all the components are in solid state and the driving force for the sintering is excess surface free energy On the contrary, liquid phase sintering is characterized by the presence of one or more than one liquid phase throughout or in a part of sintering cycle. Transient liquid phase sintering (TLPS) and super solidus liquid phase sintering (SLPS) are the variants of liquid phase sintering.

In transient liquid phase sintering liquid exists for a certain length of time during the sintering cycle. In many material systems, starting a sintering cycle with a mixture of powders will allow a transient liquid phase to form during sintering. A common example is mixed copper and tin powders, wherein tin melts at 232°C [18] The molten tin dissolves into the copper to leave behind a pore. Because tin is soluble in solid copper, the molten state persists for a short time before homogenization forms solid bronze.

In supersolidus liquid phase sintering, the sintering temperature is kept in between solidus and liquidus lines as shown in Figure 2.4. SLPS is an attractive approach for processing prealloyed powders and is extensively used in the powder metallurgy industry Figure 2.5 shows the schematic diagram of different stages of super solidus liquid phase sintering. However, a practical difficulty lies in process control, especially with respect to the acceptable temperature range for sintering. In many alloy systems, a temperature window is extremely narrow (10-20°C above the solidus) [19,20]. In addition, the interaction between process parameter such as

heating rate and sintering time, and material parameters such as powder chemistry, particle size, and grain size are important.

Sintering Pathways

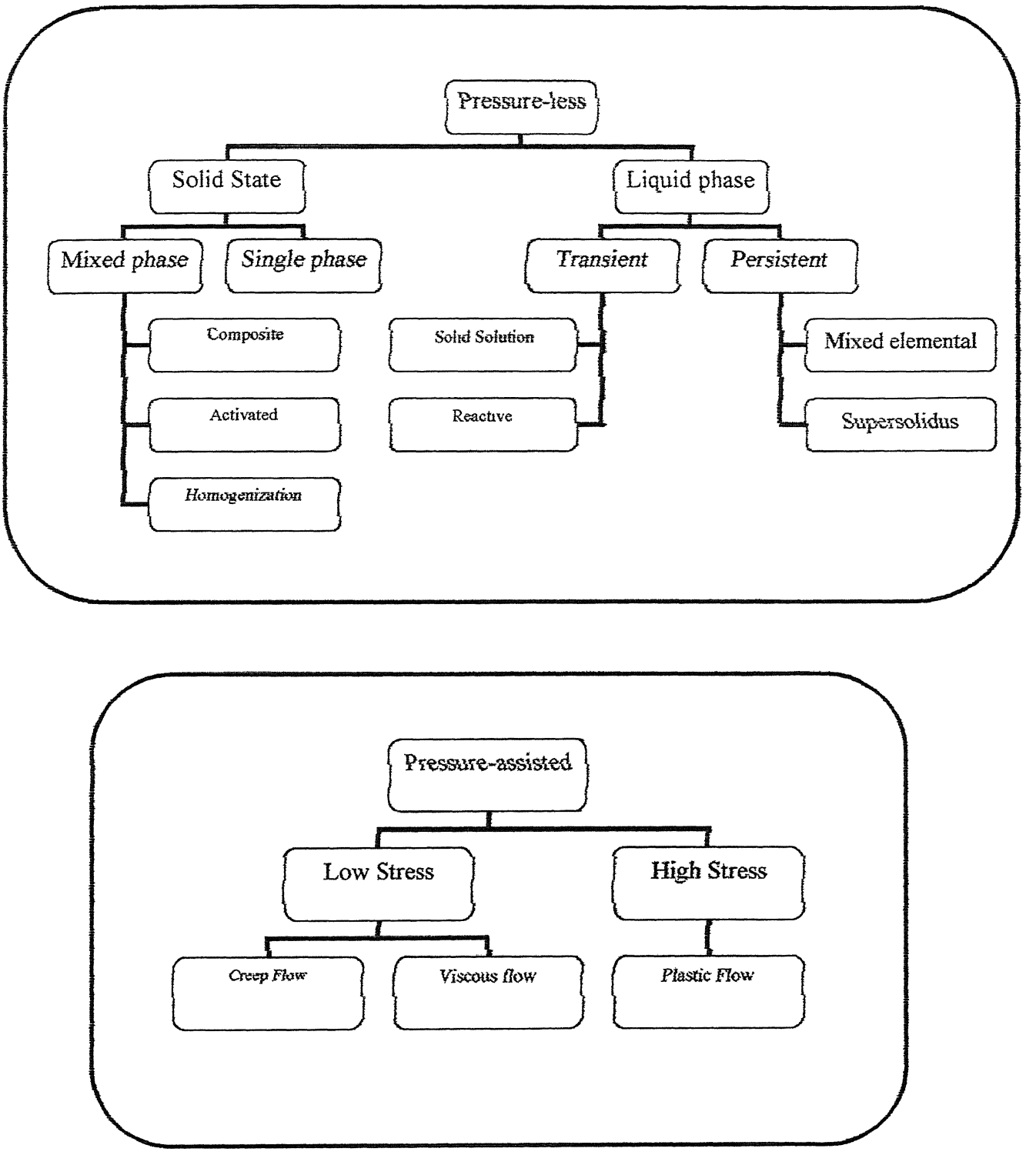

Figure 2.3 Map of sintering process and the subdivisions in terms of the key processing parameters [17].

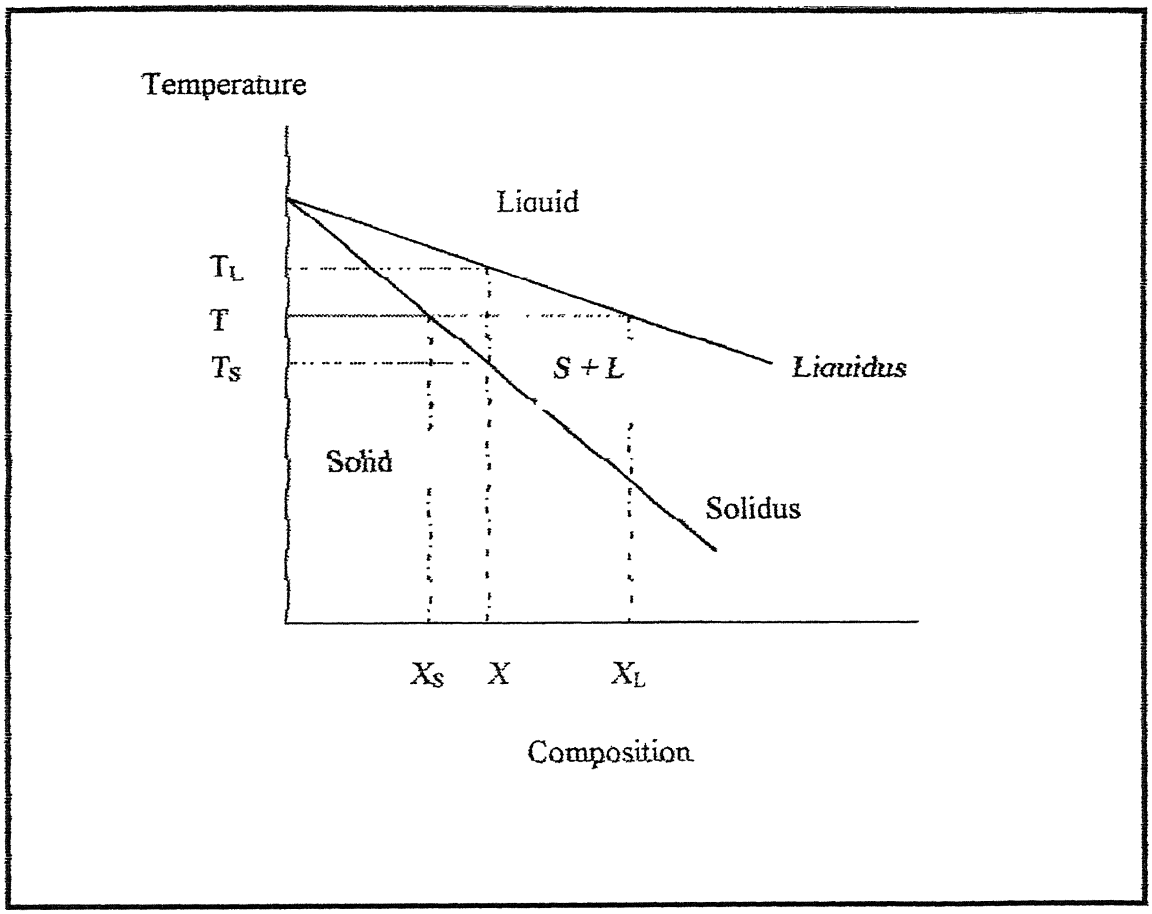

Figure 2.4 Schematic phase diagram showing different temperature of sintering

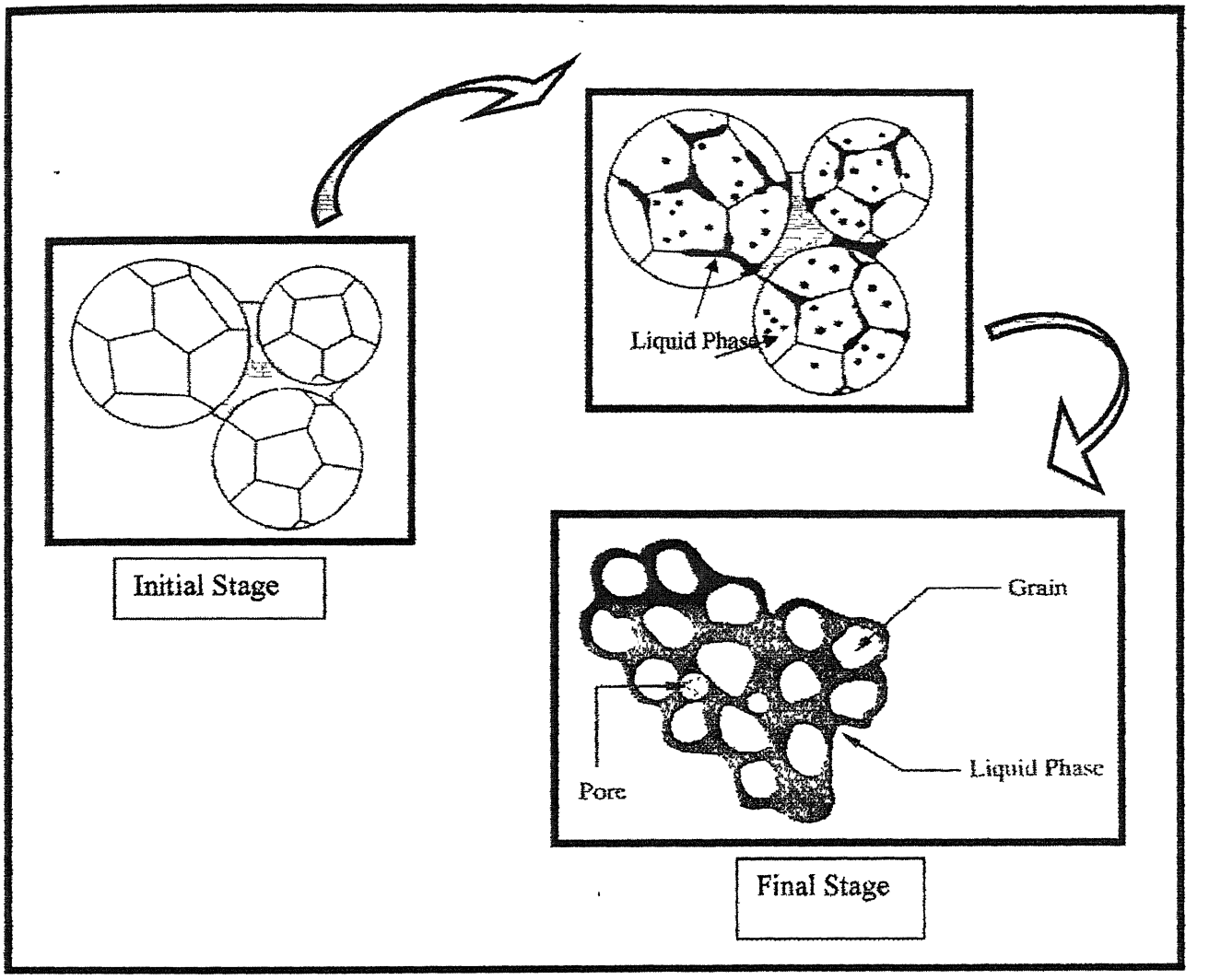

Figure 2.5 Schematic diagram of densification process during supersolidus liquid phase sintering [21].

2.4.1 A Review of Super Solidus Liquid Phase Sintering

The term "Super Solidus Liquid Phase Sintering" was coined by Cambel and Lund [22,23] in the early 1970s An essential identical approach termed as "Pressureless Sintering" was used by Lawrence and Foster [24] for Al alloy powders Still earlier, Westerman [25] reported work on the rapid sintering of prealloyed Ni-based super alloy powders at temperatures where partial melting occurred.

First attempts at explaining the sintering mechanisms during SLPS were made by Lund and Bala [26] Using Fe-0.9%C steel and Ni-50%Cu, the postulated the particle rearrangement, couple with grain shape accommodation and solution reprecipitation resulted in densification at a low volume fraction of liquid. In a subsequent study of the Cu-30%Ni system, Bala and Lund [27] also reported that particle fragmentation occurred during SLPS. However, no experimental evidence was provided.

Guyard *et al.* [28] studied the SLPS of Co-based alloy and showed that the volume fraction of liquid was dependent on the particle size. They also pointed out that coarse powder formed more liquid at lower temperatures due to incipient melting of segregated species The extent of segregation is resulted from the difference in under cooling experienced by powders of different sizes during the atomization process.

Takajo and Nipta [29] postulated that SLPS involves grain fragmentation, similar to that shown in Figure 2.5. In addition, they also reported that both densification and microstructure are dependent on the sintering temperature and time.

Using quenching techniques, Murley and German [30] experimentally demonstrated the concept of grain fragmentation using prealloyed bronze and Ni-

alloys. The result showed that both alloys exhibited different liquid nucleation sites and, hence, fragmentation behavior. However, the mechanism of particle fragmentation was not detailed. More recently, German [19,31,32] provided the first quantitative model for SLPS based on rheocasting observations. According to German's model, densification during SLPS in analogous to a viscous flow of the solid liquid mixture above a threshold temperature Although the model is conceptually sound, the inter dependence between the processing parameters is not clearly evident. Numerous studies [33-38] have used SLPS to obtain near theoretical densities in short processing times (about 60 min.). The main parameter investigated has been the sintering temperature for a given alloy composition.

Few studies have also report the grain growth behavior using prealloyed powder [37,39,40]. It has been inferred that grain growth is rapid above an optimum temperature. In addition, these studies have also shown that the grain growth kinetics is also dependent on the sintering atmosphere and the alloy chemistry. However, the grain size measurements have merely been used as qualitative indicators of the fact that the temperature control is critical in SLPS.

In summary, most of the studies have focused on optimization of processing parameters of a particular alloy system. Detailed investigation into the mechanisms behind the observed phenomenon is lacking. One of the reasons is the highly complex interdependent of parameters such as heating rate, liquid volume fraction, sintering temperature, sintering time, and powder microstructure on the densification process The next section will discuss the affect of these processing parameters on SLPS.

2.4.2 Parameters Affecting SLPS

Both material and processing parameters affect SLPS. The former includes the phase diagram characteristics and the chemical constituent of the alloy (especially with respect to the presence of additives or impurities). The later includes powder size, heating rate, sintering temperature, sintering time, and sintering atmosphere.

Liquid Volume Fraction

One of the key events in SLPS is a partial melting of a prealloyed powder to form a liquid phase. Liquid is essentially nucleated either the neck region between particles or at heterogeneous sites, typically grain boundaries within a polycrystalline particle or as isolated pools within the grains [31,41]. Each of the above mentioned liquid contributes uniquely to densification, depending on the region where it is present The liquid at the neck region provides the capillary force for rearrangement results densification. The grain boundary liquid is present as a film, and responsible for particle fragmentation. The thickness depends on the sintering temperature [42,43]. Above a critical temperature, the liquid film is sufficiently thick to initiate grain sliding due to shear stress adjacent to the neck region. The shear stress is induced by a normal stress (in this case, the capillary stress) at the neck region [44]. However, the liquid in intragranular pools is essentially trapped liquid, and hence, does not contribute directly to densification.

Densification is roughly proportional to the volume fraction of liquid. This is because the liquid phase provides the faster diffusion path in addition to a less a rigid structure, permitting easy rearrangement. The optimal quantity of liquid for densification varies from 5%-65% depending on the system and sintering condition [19]

Sintering Temperature

The identification of sintering temperature for a given alloy composition is a fundamental concern in SLPS. Because only grain boundary liquid contributes to SLPS densification, it is difficult to predict optimal sintering temperature [44]. Recent studies on SLPS [19,45] show that rapid densification above a critical temperature occurs due to viscous flow of the solid grains in a liquid matrix. With an increase in temperature, the viscosity of the solid liquid mixture is reduced largely due to an increase in liquid content, thus enhancing densification kinetics. On the other hand too high a sintering temperature results in degradation of mechanical property due to excessive grain coarsening [39,40,41,46], besides leading to compact slumping. Typically, the transition from an under sinter to a fully sintered state occurs over a narrow temperature interval. In many cases, the sintering window is narrow (10-20°C in the vicinity of the solidus temperature). Thus for any alloy system the sintering temperature has to be optimized for a given starting particle size and heating rate.

Sintering Time

The optimum sintering time is determined by the sintering temperature. For example, if sufficient liquid exists (around 25-30 vol %), then complete densification can be achieved by the rearrangement process alone [47-48]. In this case, the sintering time can be as low as 10-15 min [29] Alternatively, a lower sintering temperature implies less liquid; hence time dependent mechanism such as solution reprecipitation, grain shape accommodation, and pore removal are required to attain full density. However, this longer holding time generally leads to coarser grain and thus decrement of the density.

Sintering Atmosphere

The choice of sintering atmosphere does not affect the sintering mechanism but affect the degree of densification and the resulting mechanical properties. The gas used as sintering atmosphere can be entrapped in pores and inhibits densification during the final stages. Often the limiting density is higher for sintering in hydrogen, which dissolves in many metals, than in inert gasses like Ar. Vacuum sintering avoids trapping gas in the pores and subsequent pore swelling. Ultimately the choice of sintering atmosphere depends mainly on the alloy system, in addition to economic consideration.

Powder Characteristics

Powder characteristics such as initial powder microstructure, shape and size have also an important role to play in SLPS. As stated earlier liquid may form at the grain boundaries or inside the grains, i.e. in the interdendritic regions. A cellular structure is preferred over a dendritic structure since liquid at the grain boundaries leads to grain refinement and sliding thus contributes directly to densification. On the other hand the intra granular liquid pools do not have significant effect on densification. SLPS is thus generally done with the prealloyed powder fabricated through gas atomization route.

SLPS works with relatively coarse powders. This is an advantage in comparison with classic liquid phase sintering which uses mixed elemental powders near 1 μm. Coarse powders have less contamination and easier to handle. Nearly full density can be attained with powders as large as 500 μm. However, smaller particles give more initial densification specially at temperatures below the optimal. At the

optimal temperature there is little particle size role. As a practical limit, a mean particle size of 80 μm for smaller is reasonable for many systems [49]

Heating Rate

The heating rate is dictated by the furnace capabilities and a need to reduce surface oxides prior to significant densification Depending on the particle size, there may be little solid-state densification prior to the formation of the first liquid. This differs from classic liquid phase sintering using small particles where up to 90% of the densification occurs by the solid state diffusion prior to liquid formation. Slow heating rate allows sufficient time for grain coarsening and reduces the compositional gradient, giving less densification at temperatures below the optimal sintering temperature. On the other hand, faster heating rate gives faster densification in SLPS since less homogenization occurs [19,50].

Alloy additives

Impurities or alloy addition segregated at the grain boundaries can alter the liquid formation temperature and amount of liquid. Intentional additives help control liquid formation in and between particles and widen the temperature range for sintering [19]. In addition, to activating densification during sintering some of the sintering additives play a significant role in final mechanical and corrosion properties [51].

As an example, boron mixed with prealloyed cobalt alloys will induce a surface liquid early in the SLPS cycle and improve process control. Elemental nickel has been mixed with nickel-base superalloys to expand the temperature range over which densification occurs. Also oxides or other inert inclusions retard microstructural coarsening [19].

Phosphorus has a well known beneficial influence on the strength of tin bronze promoting a uniform and fine grained texture in alloy. A small amount of phosphorous (0.1-0.4%) widens the solidification range of tin-bronze considerably and it also lowers the viscosity of the melt appreciably [14].

2.4.3 Limitations of SLPS

In spite of all the advantages, supersolidus liquid phase sintering suffers from certain disadvantages some of which are inherent of liquid phase sintering. These are as follows:

i. The major problem is the compact distortion. It may occur due to the formation of too much liquid during sintering. The large dimensional change which occurs during sintering puts limits on dimensional tolerance [52].

ii. The alloying level should be reasonably high on a volume basis to aid in maintaining segregation in the particles and to help the widen separation between the liquidus and solidus temperatures.

iii. At the candidate sintering temperature, which corresponds to approximately 20-30 vol. % liquid, the separation between the solid and liquid compositions should be moderately large. This minimizes the effect of slide compositional fluctuations and diminishes the sensitivity to sintering temperature.

2.4.4 SLPS of Bronze

Copper-tin alloys (tin bronze) are remarkable for their favorable combination of high hardness and ductility values with good corrosion resistance. However, the demand for corrosion resistance non-ferrous materials harder and stronger than the

standard sintered brasses or tin bronzes made from premix route has stimulated interest in the use of prealloyed powders Prealloyed bronze powders are produced by melting the constituents copper and tin to form a homogeneous alloy and atomizing the alloy melt by either gas atomization or water atomization Here solute atoms (Sn) substitute for solvent atoms (Cu) to give a single phase α-solid solution having the face centered cubic crystal structure of the Cu atoms, thus increasing the strength (yield strength, tensile strength and hardness) by solid solution strengthening. The increase in strength is a function of the alloy composition and of the size difference between solvent and solute atoms. The most effective hardening arises from Sb, In or Sn in which the atomic radii are considerably higher than that of Cu. Typically the substitutional alloying gives rise strength increases by a factor of from 2 to 5 [53].

A wide compositional range of prealloyed bronze are available, these materials are used primarily in the fabrication of structural parts where higher densities is desirable for improve mechanical properties. However, prealloyed bronze powder suffers from their nodular particle shape and high apparent density result in low green strength. This problem has been overcome by allowing the part to achieve the require density through densification during sintering which permits the use of lower compacting pressures.

Dowson clearly indicated [54] that in equilibrium condition tin is soluble in copper lattice at least 15 wt.% in the temperature range of 500°C to 600°C. At those temperatures Cu-10/12 Sn would consist of single α phase. But at lower temperature solubility of tin decreases and below 340°C second phase should begin to appear. Decomposition of α phase requires extremely slow cooling rate. But industrially it is not possible all time. So, in final microstructure we can get the phases which may not

be supported by phase diagram. Krishnakant *et al* [55] reported that prealloyed powders in premix formulations helps to produce bearings with less distortion Collur and Upadhyaya [56] investigated sintering of 9 wt% tin bronze containing 0 to 3 wt% iron at different temperature obtained both through premixed and prealloyed routes They showed sintering through premix route exhibited growth and relatively lower hardness values while opposite is true for prealloyed route They also indicated that iron addition in bronze up to 1 wt% enhances the densification of premix powder while the reverse is true for prealloyed compacts. According to their investigation ternary tin bronze attend maximum densification after sintering at 800°C, process through either route.

Chapter 3...

SCOPE OF THE PRESENT WORK

SCOPE OF THE PRESENT WORK

From the previous chapter, it is evident that bronze plays an important role in the fabrication of many industrial parts ranging from porous bearing to full density structural parts. One of the most important routes of making those products is through powder metallurgy technique. The justification of selecting powder metallurgy as a manufacturing process for bronze products can be cited as follows

i. Good enough difference in the melting point (1083°C of Cu to that of 232°C of Sn).

ii. As bronze system can be sintered within 1000°C, handling with the furnace would be easier.

iii. Powders of all size and shapes can be economically fabricated and available commercially.

iv. Powders compressibility is good as compared to refractory and other ferrous metals.

v. Not that much highly sensitive to the requirement of reducing gases, and therefore sintering can be done in forming gas well which is much cheaper.

vi. As bronze is widely used in fabrication of porous material, such as bearing and filters, distribution and control of porosity are easier through P/M route compare to any other production route

Both solid and liquid phase sintering are applicable towards the production of near-net shape product from bronze. Currently, about 70% of the total sintered products are being produced by liquid phase sintering [2]. Various novel sintering techniques have also been attempted for the processing of P/M bronze. However,

bronze has primarily been processed by solid state sintering alone. This is partly attributed to the requirement of the end applications, i.e. bearing wherein a controlled porosity is required. Recently, there has been a considerable attempt to use P/M bronze and bronze-based composites for structural applications, wherein achieving high density is a primary requirement. To achieve this full density liquid phase sintering would be the best alternative. Unfortunately, the potential of the use of Cu-Sn bronze as a structural material have not been fully explored while parts made from other copper alloys, such as brass, leaded brass, and nickel silver are produced from prealloyed atomized powder.

Cu-Sn system is relatively well known and has been investigated over the years. It is also known that this particular system can be used for the production of porous bronze bearing. Production of self-lubricating Cu-10Sn bronze bearings has been underway since the 1920's and these still constitute a major use for copper and tin metal powders. It was observed that the P/M route for processing bronze bearing offers many advantages compared to the other processes, as has been described in the previous chapter. Such bearings were used to be manufactured by solid state sintering only. When the historical background of bronze bearings is reviewed, it appears that the ground work was initiated at Chrysler-Amplex and Delco-Moraine in the 1920's. In order to satisfy their powder needs, Everett Hall established the pioneer company – Metals Disintegration [55]. A good review of sintering work on copper and tin was reported by Hall [57]. But the basic mechanisms of liquid phase sintering were unknown at that time. It was in the late '70s, when the people focused attention to the logical aspects of liquid phase sintering of bronze. Nowadays both prealloyed and premixed powders are used in the industries. The advantages offered by LPS provided

the driving force to the researchers for investigating the liquid phase sintering mechanisms of this system.

Dowson [54] discussed the sintering aspect of bronze in a concise fashion, taking into consideration the relevant phase diagram. His work clearly shows that in equilibrium condition tin is soluble in copper lattice up to at least 15 wt. % in the temperature range of 500°C to 600°C. At that temperature Cu-10/12 Sn would consist of single α phase. But at lower temperature solubility of tin decreases and below 340°C second phase should begin to appear Decomposition of α phase requires extremely slow cooling rate But industrially it is not possible all the time. So, in final microstructure we can get the phases which may not be supported by phase diagram.

The sintering operation is believed to be affected by powder characteristics, sintering atmosphere, compact density, rate of heating etc. [54, 55]. Lower apparent density and smaller particle size would lower the growth. Lower the density of green compact, lower will be the growth Greater reducing potential of the gas also lowers the rate of growth. To minimize the growth, lower heating rate is adopted.

Pore content in the sintered product varies from 20 to 40% by volume. Larger the pore content, oil impregnation is more and that is helpful in case of self lubricating bearing. But strength factors also should be considered. Optimization between the strength and porosity is done depending on application. However, if prealloyed powder is used, sintering and dimensional control are relatively easy, but the problem is, the temperature needed for sintering will lead to shrinkage which is not desirable for bearing Furthermore, prealloyed bronze particles are harder than pure copper, therefore greater pressure is needed.

Krishnakant *et al.* [55] also reported that prealloyed powders in premix formulations helps to produce bearings with less distortion The surface of fully sintered bearings is often less smooth and may contain high spots. Some of these may still be present after sizing, which add to the noise and inferior performance of a bearing. In such instances, higher percentage of prealloyed powders in premix formulations was found to help retain the surface smoothness. Berry [58] had studied the role of prealloyed powders in various mixtures along with other factors influencing the dimensional changes.

Premixed powders are seen to provide linear growth as high as 4%. Other complication is that growth is not the same in radial direction as in the axial direction.

Deegan and Sarkar [59] discussed the effect of compacting pressure and sintering temperature on the properties of copper-tin compact upto 10% tin. The sintering time was kept to maximum 15 min. Within this temperature range, progressive volume growth was observed. More the tin content, more the growth At higher compacting pressure, with increasing tin content greater ejection force required for the compacts. It is possible that, at high compacting pressure, the tin will flow plastically over the die wall and the junctions so formed are strong, offering resistance to movement of the compact.

Backensto [60] studied the changes in dimensions during the sintering of bronze mixes made from reduced copper. Among the variables investigated were copper particle size, tin content, tin particle size, lubricant variations, effect of graphite additions, and effect of lead and phosphorus additions. They have also reported that within the sintering time limit the dimensions at first increase and then

decrease for further temperature increase. After sintering at around 850°C, good α bronze microstructure with good strength, ductility, and machinability were obtained

Berry *et al.* [61] had studied the change in dimensions during heating up to sintering temperature. The common practice of decreasing sintering temperature for dimension control adversely affects machinability and bearing performance.

Since there is an interest in using bearings containing tin greater than 10%, the effect of tin on properties of pressed and sintered compacts containing tin upto 20% was investigated by Davies and Sarkar [62]. They suggested that shrinkage occurs by solid state sintering of bronze beyond a critical sintering time dependent on the temperature Diffusion, which is temperature and time dependent, during sintering causes alloying and the system undergoes shrinkage due to solid state sintering.

Research results on mixes containing various combinations of prealloyed and/or elemental tin powders in combination with reduced/unreduced copper powders were published by Peissker [63]. Mukunda *et al.* [64] studied the vacuum sintering of bronze bearings in light of interconnected porosity, sintering parameters and green densities. They selected reduced, electrolytic and atomized copper powders of varying particle sizes. It was suggested that the amount of interconnected porosity is dependent on some ratio of the copper and tin particle sizes. Vacuum sintering was found to offer a slight improvement in the interconnected porosity. The effects of various green densities on the flow of tin into the capillaries and homogenization of the microstructure were summarized by Kim [65]. They selected spherical tin powders of average particle sizes of 30, 65, and 140 μm, while copper powder was irregular shape sieved to a 20 to 60 μm size range. Sintering was carried out at 400°C for 10 min in hydrogen. The results showed that the flow of the tin-rich melt depends

critically on the green density. When the green density was high, the tin-rich melt remained at the initial tin particles and the resulting compositional and structural inhomogenity persisted even after long sintering at high temperature. On the other hand, when the green density was low, the tin melt spread into the capillaries, thus facilitating a homogeneous microstructure. But since pores are produced at the tin particle sites, it is also desirable to control the tin particle size and its distribution.

Das *et al.* [66] have studied extensively the control of δ phase in 90/10 bronze bearing. Improper sintering may give rise to brittle tin-rich delta phase in the form of (α +δ) eutectoid. According to them the brittle phase can be controlled by any one or a combination of the following:

(i) Increased sinter temperature.

(ii) Increased sinter time.

(iii) Part or total replacement of elemental copper and tin powder by prealloyed bronze powder.

But none of the above alternatives proved satisfactory because every alternative has got its own limitations. At the same time it should be noted that, water atomized prealloyed bronze powder is capable of producing a fully developed microstructure which is free of delta phase when sintered properly They conducted the experiments with three kinds of powders: elemental mixture of Cu and Sn, mixture of prealloyed bronze, 45% Cu and 5% Sn, and 100% prealloyed bronze. Sintering was carried out at two different temperatures, 750°C and 790°C. Compacts made from elemental mixtures of copper and tin showed combination of α and δ phases in the microstructure. But all of the three different powder compacts showed only homogeneous α phase after sintering at 790°C for 30 minutes. This implies that

by proper selection of sintering temperature and time we can achieve desired α phase in the final microstructure.

Mukunda *et al.* studied the sintering process in the copper-tin system elaborately and published the results in a series of papers [67-69] They also discussed the prevalence of two schools of thought. In one it is believed that copper diffuses into tin to from various intermetallics which either decompose or get transformed into less-tin-rich phases as the sintering progresses. The other believes that tin melts and spreads, leaving behind secondary pores of approximately the same size and shape Farmer [70], on the other hand, has formulated an entirely different scenario in which molten tin begins to diffuse into copper to form extremely small grains of bronze, which later coalesce to form larger grains. Mukunda *et al.* [67] studied in detail the formation of structure in the compact made from premixed copper and tin when heated from room temperature to 850°C. They also investigated the variables affecting the sintering operation Atmosphere limitations were obvious in their investigations as they selected only argon or nitrogen. As such, their studies are not useful in real sintering practice, but the authors have covered excellently the microstructural features during sintering. They have also described the synthesis of various phases and intermetallics and their identifications [71].

Messener *et. al.* [72] studied the effect of the copper powder on the liquid phase sintering process. Two different copper powders were considered: one electrolytic and the other atomized. The copper/tin interaction is influenced by the surface oxidation of the powder particles and by the surface area. This influences the homogenization of tin in the copper matrix and the amount of the liquid phase and, in turn, the dimensional behavior of the systems.

Menapace *et. al.* [73] studied 90/10 bronze bearings which were produced by sintering two different copper powders, one atomized and one electrolytic. Sintering was carried out at different temperatures and times in order to study the effect of these parameters on the microstructural characteristics, pore morphology and mechanical properties

The most recent study on sintering of bronze has been reported by S. Ghosh [2]. He worked on Cu-12%Sn premixed and prealloyed bronze through transient and supersolidus liquid phase sintering. He clearly showed that premixed and prealloyed powders behave separately during sintering. Premixed samples exhibited expansion at a lower temperature than prealloyed sample. He also concluded that prealloyed samples led to higher densification when sintered through SLPS compare to solid state sintering. If the bronze is to be used for bearing applications, premixed powders are more suitable than the prealloyed one Expansion of premixed compacts gives rise to interconnected pores which will be able to contain the oil during service condition. On the other hand, for structural applications prealloyed powders seem to be the best route.

Until now, most researchers have dealt with mainly Cu-Sn elemental powders for making P/M bronze products Not much effort has gone into systematically identifying the behavior of prealloyed bronze powders during sintering. In the literature not much work related to application and use of prealloyed powder was found. Considering the two above factors into account, it can be concluded that sintering of prealloyed bronze powders through supersolidus liquid phase sintering will be an interesting approach. So far no such work has been reported on Cu-Sn

prealloyed bronze material produced through powder metallurgy route. Considering this fact it was considered worthwhile to study this material

From effective and economic point of view, it would be worthwhile to select, before starting experiments, alloy composition, sintering parameters such as sintering temperature, sintering time, sintering atmosphere, etc. Literature survey reveals that tin is soluble in copper up to 15 wt %, even at room temperature, giving only the single phase α in the microstructure, which may not be supported by the phase diagram [54] Literature reviews also show that the widely used bronze powders in the powder metallurgy route contain generally 9-12 wt. % of tin. From the phase diagram of Cu-Sn [Figure 2 1], for Cu-12 wt. % Sn the first liquid is formed at 820°C. Considering all these, in the present investigation, the composition Cu-12%Sn has been selected, whereas temperatures of 830°C upwards were considered for sintering. Early researchers selected total sintering time within the hot zone ranging from 15 to 60 min. In the present case a single sintering time of 60 min has been selected It is necessary to select sintering atmosphere judiciously because densification is largely dependant on sintering atmosphere. Hydrogen has been selected for this purpose, because its reducing capability not only provides protection from further oxidation but also can reduce any existing oxides. Many other researchers have tried H_2 for this reason.

It is further aimed to study the properties and microstructural details of the sintered products using proper characterization methods Microstructural evolution has been studied as a function of sintering temperature and compacting pressure. Optical microscopy has been used to observe the phases present in the microstructure and the distribution of pores in the matrix. Macroscopic dimensional variations have

also been found out by the measurement of dimensions in both axial and radial directions XRD studies have also been made to confirm the presence of phases in the final microstructures.

Chapter 4...

EXPERIMENTAL PROCEDURE

EXPERIMENTAL PROCEDURE

4.1 Raw Materials

4.1.1 Prealloyed Powder

The alloy chosen for this study was water atomized prealloyed 88Cu-12Sn (wt %) bronze. It was procured from SCM, NY, USA. The chemistry of the sample is simple i.e without any surface oxide and shape was near spherical.

4.2 Powder Characterization

The as-received powders were characterized for their size, distribution and morphology. Most of the characterization techniques require only a small quantity of the sample powder; it is therefore assumed that the powder sample is representative of the bulk.

4.2.1 Particle Size and Distribution

The data on particle size and distribution have been taken from the original work by S. Ghosh [2]. Powder size measurement was accomplished using a laser-scattering size analyser (model: Economy, Laser Klasse 1; supplier: Fritsch, Germany). Low angle Fraunhofer light scattering using monochromatic (laser) light and dispersed particles are used in this case. Particles are suspended in a moving fluid. The suspension was made using 1 to 3 g of powder in approximately 60 ml of distilled water with 10% sodium metaphosphate. The particles are passed through a laser beam in a circulating water stream. The light is scattered after the interaction with the particles, and the intensity is measured by strategically placed detectors. Particle size affects both the intensity and

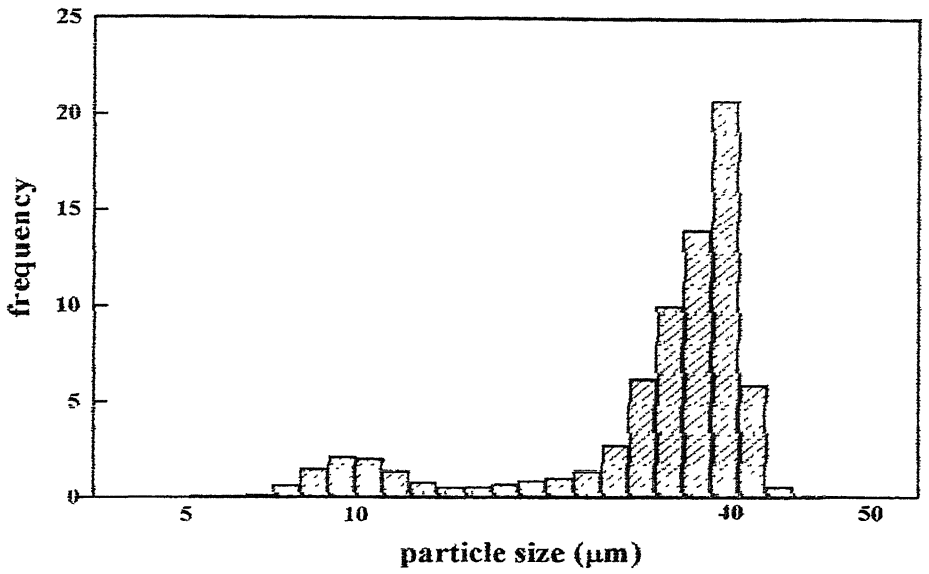

Figure 4.1 A histogram plot of the particle size analysis of prealloyed powder. Particle size axis is on a logarithmic basis

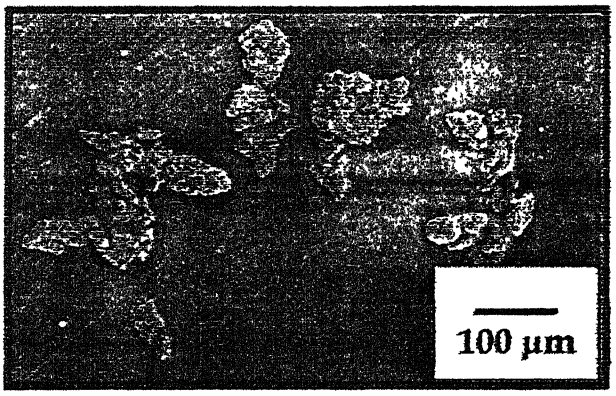

Figure 4.2 SEM micrographs of prealloyed Cu-12Sn powder.

angular extent of scattering With coherent light the angle of scattering varies inversely with the particle diameter The scattering depends on the refractive index of the particle in the suspending medium, the wave length of light and the particle size and shape Figure 4.1 shows the particle distribution of prealloyed powder. That plot shows a bimodal distribution. Maximum number of particles was in the range of 35-40 μm size.

4.2.2 Particle Shape

A qualitative measure of particle shape was obtained using a JEOL, JSM – 840 A, Scanning Electron Microscope, in the secondary electron (SE) mode. The SEM permitted far greater viewing magnification than optical equipment. As shown in SEM image of Figure 4.2, the as received Cu-12Sn prealloyed powder has nearly rounded appearance and was fabricated by water atomisation.

4.3 Compaction

Cylindrical green compacts of 12.7 mm diameter and approximately 3 mm to 5 mm height were made from prealloyed bronze powder using a CTM-50, SRN 6/93-1800, compression testing machine supplied by Fuel Instruments & Engineering Private Limited, Ichalkaransi, Maharastra, India. The die made of high chromium high carbon steel was cleaned with acetone and was lubricated with zinc-stearate prior to each powder fill. Lubrication facilitates subsequent removal of the compacted samples. In this study, two extreme pressure conditions were chosen for compaction. The compacts were pressed at 150 MPa and 600 MPa.

4.4 Sintering

Sintering was carried out in a laboratory made SiC-heated horizontal tubular furnace (rating 1.5 kVA). The furnace tube was made up of doubly recrystallized alumina. The inner diameter of the tube was 38 mm and length 980 mm. Sintering was done in commercially pure hydrogen (dew point: -35°C) atmosphere. The flow rate of hydrogen was maintained at 1 l/min. The furnace had a heating zone of approximately 105 mm in the temperature range of 1250°C – 1350°C with an accuracy of ± 5°C.

In the present study five different temperatures were selected for sintering. The temperatures were 775, 830, 860, 890, and 920°C. The sintering at 775°C was done by S.Ghosh for his M.Tech thesis work. [2]. In this study, his experimental data have been incorporated. For rest of the samples, requisite numbers of green compacts were placed over an Inconel boat and transferred in the centre of the tubular furnace. Inconel has got a much higher melting point than the maximum sintering temperature used. This will avoid any sticking problem of the samples with the boat. Both ends of tubular furnace were sealed with SILASTIC (RTV 700) adhesive/sealant to prevent any leakage. Heating rates were same for all the sintering operations (5°C/min). The samples were heated to the final sintering temperature without intermittent holding. Holding time was 60 min at final sintering temperature for each case. Automatic temperature controller was used to control the temperature within ± 5°C. In all cases cooling was done in prevailing atmosphere, i.e. furnace cooling, at an average rate of 2 –3°C/min. All the sintering data are provided in a tabular manner in Table 4.1.

Table 4.1: Types of sintering at different temperatures.

Sintering Temperature (°C)	Compaction Pressure	State of Sintering
775	150	SSS
	600	SSS
830	150	SLPS
	600	SLPS
860	150	SLPS
	600	SLPS
890	150	SLPS
	600	SLPS
920	150	SLPS
	600	SLPS

SSS: - Solid State Sintering

SLPS: - Supersolidus Liquid Phase Sintering

4.5 Densification Behaviour

4.5.1 Density and Densification Parameter

Densities of the green cylindrical compacts were calculated from the mass and physical dimension measurements of the samples whereas the densities of the sintered samples were calculated either by the previous method or by Archimedes principle Densification parameter was also a way to determine the amount of densification that has occurred after sintering. Densification parameter (ψ) was expressed as follows

$$\psi = \frac{SD - GD}{TD - GD}$$

where SD is the sintered density, GD is the green density, and TD is the theoretical density.

4.5.2 Linear and Radial Shrinkage

Linear dimensions of the sintered samples were measured using vernier callipers and screw gauge. Average of four measurements of each dimension is reported. The formula used for calculations are as follows,

$$\delta h = \left(1 - \frac{h_s}{h_g}\right) \times 100\%$$

$$\delta r = \left(1 - \frac{r_s}{r_g}\right) \times 100\%$$

Where,

h_g, r_g → height and radius of the green compact

h_s, r_s → height and radius of the sintered compact.

δh → % linear shrinkage in height

δr → % radial shrinkage

4.5.3 Xylene Method for Porosity Determination

The specimens, immersed in xylene, were placed in a vacuum desiccator and the pressure was reduced for a period of 20 min by a pump. This treatment removed gas from the open pores and allowed the xylene to enter into them. The specimens were then taken out from the xylene, and after the surface liquid had been wiped off by means of filter paper, they were weighed in air and in water The xylene being non-miscible with water prevented the water from entering into the pores, so that the difference between the last two weighing gave the total volume of the specimen [74].

Letting A_1 = weight of the specimen, B = weight of the specimen after impregnation with xylene, and C = weight of the impregnated specimen in water·

B – C = volume of specimen

$$\varepsilon_1 = \frac{(B - A_1)}{(B - C)\rho_x}$$

$$\varepsilon_T = \frac{(B-C) - \frac{A_1}{\rho_{Cu-12Sn}}}{(B-C)}$$

$$\varepsilon_T = \varepsilon_1 + \varepsilon_C$$

where ε_i and ε_T are the interconnected and total porosities, respectively, and ρ_x and $\rho_{Cu\text{-}12Sn}$ are the densities of xylene and bronze The difference between ε and ε_i gives ε_c, the closed porosity

4.6 Macro structural Studies

Photographs of sintered samples were taken by the help of a digital camera made by Fuji, Japan

4.7 Micro structural Studies

4.7.1 Optical Microscopy

Sintered samples were cut from the middle so that their cross section can be open up and then cold mounting was done. The compacts were wet polished on the Lunn Major Unit made in Struers, Denmark make 220, 320, 500 and 1000 grit silicon carbide emery papers followed by fine wheel polishing with suspended 0 03 μm size alumina in distilled water. Acidic $FeCl_3$ was used as the etchant. Composition of the etchant was:

$FeCl_3 \rightarrow 5$ g

$HCl \rightarrow 50$ ml

$H_2O \rightarrow 100$ ml

Etchmg was done on the leather for 15-20 s. The microstructure was exammed using Leitz Labor Lux 12Mes Image Analyzer.

4.8 Mechanical Properties

4.8.1 Vickers Macro-hardness

Vickers Macro-hardness of the polished specimens was measured on Leco V-100-C1, Hardness Tester, manufactured by Akashi Corporation, Japan. The machine was automatic and time for indention was pre-programmed. The load of 300 g and indentation time of 15 s was maintained The diagonal lengths of the impressions were measured and the hardness was obtained directly in HV scale on the monitor.

4.8.2 Vickers Micro-hardness

Vickers micro-hardness had been taken at a load of 5 g on polished and etched samples in a micro-hardness tester, manufactured by Leitz Weltzlar, Germany. The indentation time of 30 s was maintained. The diagonal lengths of the impressions were measured and the hardness was obtained from the standard chart.

4.9 X-ray Diffraction Analysis

X-ray diffraction studies on the powder (both premixed and prealloyed), green and sintered compacts were carried out on Rich Seifert & Co., Germany make, ISO Debyeflex –2002 diffractometer. Powders were kept in a square holder with very small thickness. Some methyl alcohol was put on the powders so that they would be properly adhered during the diffraction study. Compacted samples after grinding up to 1000 grit SiC paper were put into the holder for analysis. The various parameters during the experiment are as given below,

$$\text{Target (Radiation)} \rightarrow \text{Cu } (K_{\Delta})$$

$$\text{Wavelength, } \lambda \rightarrow 1.542 \times 10^{-10} \text{ m}$$

Scanning Speed → 3°C/min, (in 2θ)

Counts/min → 50,000

Time Constant → 3 s

Amperage → 20 mA

Voltage → 30 kV

The X-ray machine is interfaced with computer. While scanning the sample, computer saved all the data (intensity and angle) as a text file. Those files are taken and the intensity vs. angle graphs was re-plotted by using Origin software. Analysis of those peaks was also done by the same software. Indexing of X-ray diffraction patterns were carried out by matching using computer package of Joint Commission for Powder Diffraction Standard (JCPDS), ed. 1996.

Chapter 5...

RESULTS

RESULTS

The experimental results of the present investigation are divided into seven different sections. The first section presents the result of the sintering parameters and properties of prealloyed Cu-12Sn sintered compacts. In this section density and densification parameters of the samples are discussed. Next section gives the measurement of porosity through xylene impregnation. In the third section radial and axial shrinkage behaviours are compared. Macrographs, optical microscopy, hardness testing; macrohardness and microhardness, x-ray diffraction results are given in the subsequent sections

5.1 Density and Densification Parameter

As described in the earlier chapters, in the present study we have dealt with Cu-12%Sn prealloyed system. The alloy powder was produced by water atomisation route. Appendix I and II give the experimental data before and after sintering for all the samples used in the present study It is evident from Figure 5 1 that green density increases with increasing pressure. Increasing pressure from 150MPa to 600MPa brings a change in theoretical density from 60% to 80%. Appendix II gives the effect of sintering on the density. Figures 5.2 and 5.3 show the change of green density after sintering at different temperatures for both 150 and 600 MPa samples, respectively. Figure 5.4 shows the variations of sintered density with temperature. It is seen that maximum density obtained was for the sample pressed at 150 MPa and sintered at 860°C As we increase temperature further, final density decreases, for both 150 and 600 MPa samples

Densification parameter is also very important to understand the behaviour of sample So, densification parameters are plotted for the samples and shown in Figure

5.5. It shows the effect of compaction pressure as well as sintering temperature on the densification of the samples. The behaviours are different for 150 MPa and 600 MPa samples Densification parameter is positive for 150 MPa samples up to temperature around 890°C whereas it is not the case for 600 MPa samples. It is positive for sample sintered at 830°C, but as we increase temperature, it has become more and more negative. This implies that 150 MPa samples shrink up to 890°C and thus densified. On the other hand, 600 MPa samples expand and with increasing temperature the amount of expansion also increases.

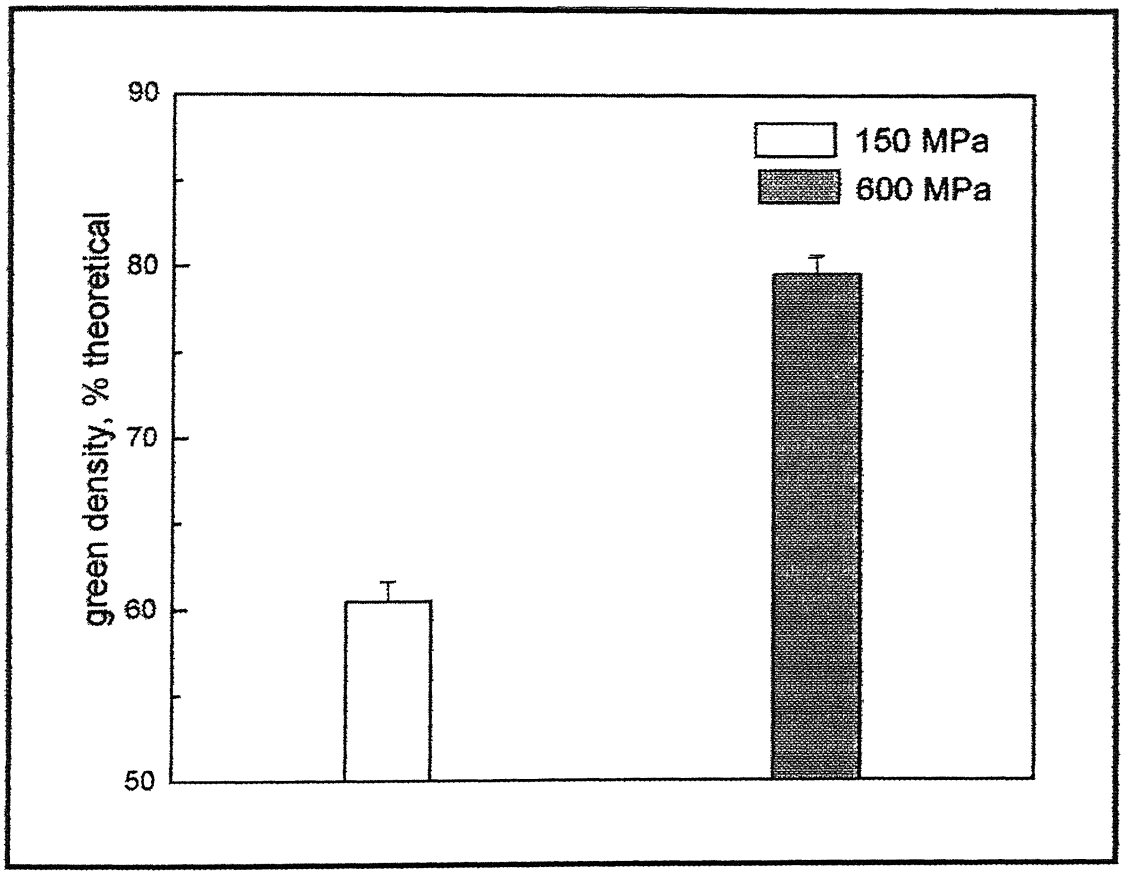

Figure 5.1 Effect of compaction pressure on green density

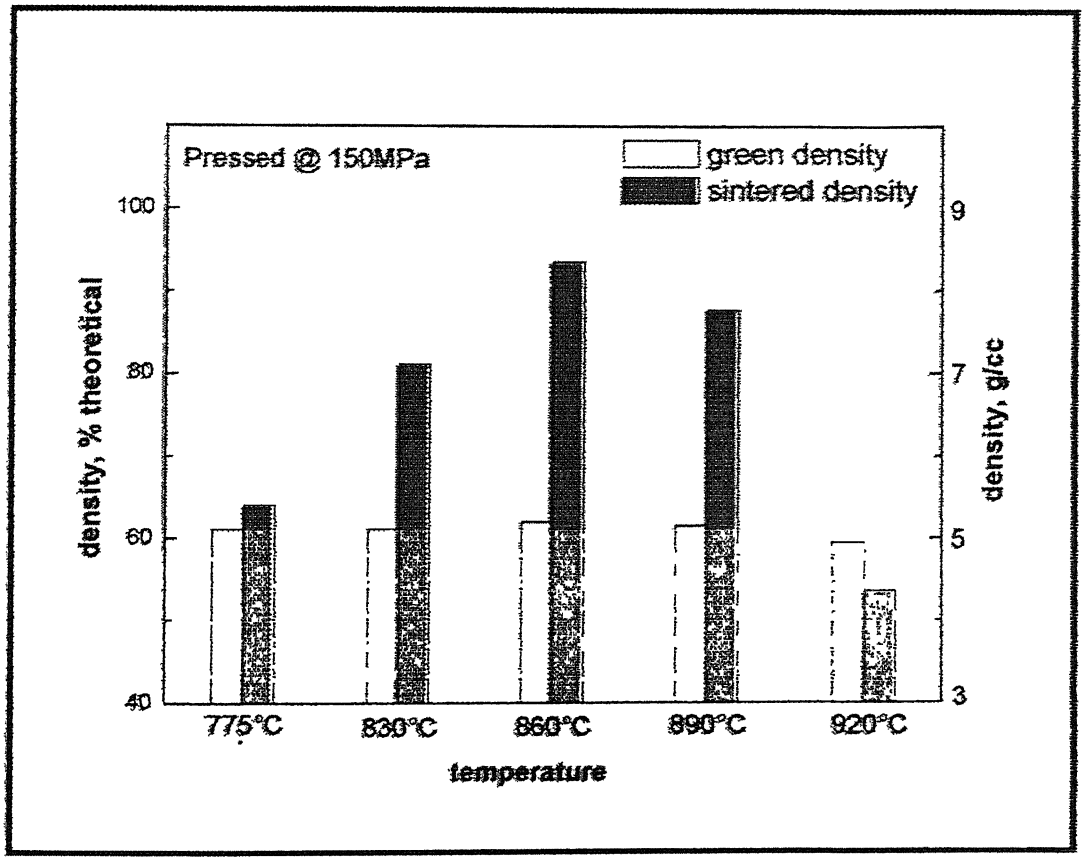

Figure 5.2 Comparison of green density and final density of the samples pressed at 150 MPa.

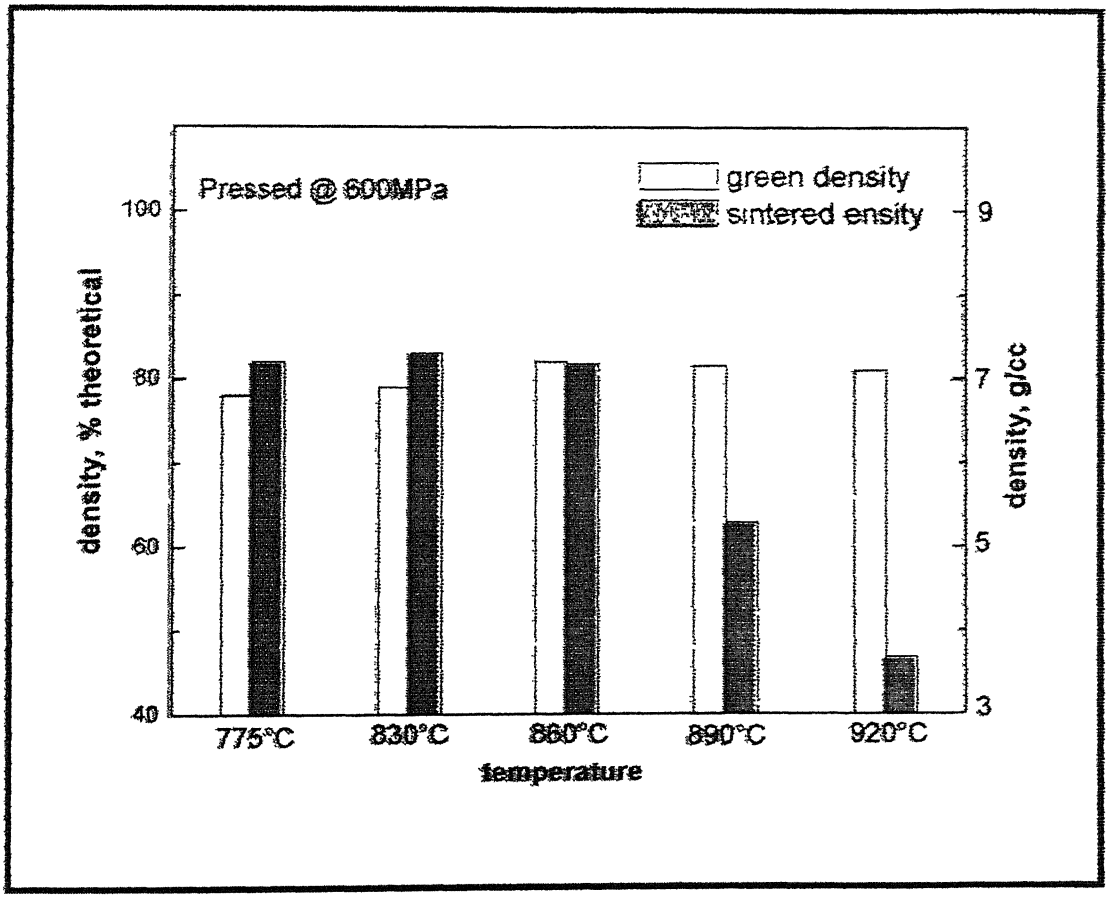

Figure 5.3 Comparison of green density and final density of the smaples pressed at 600 MPa

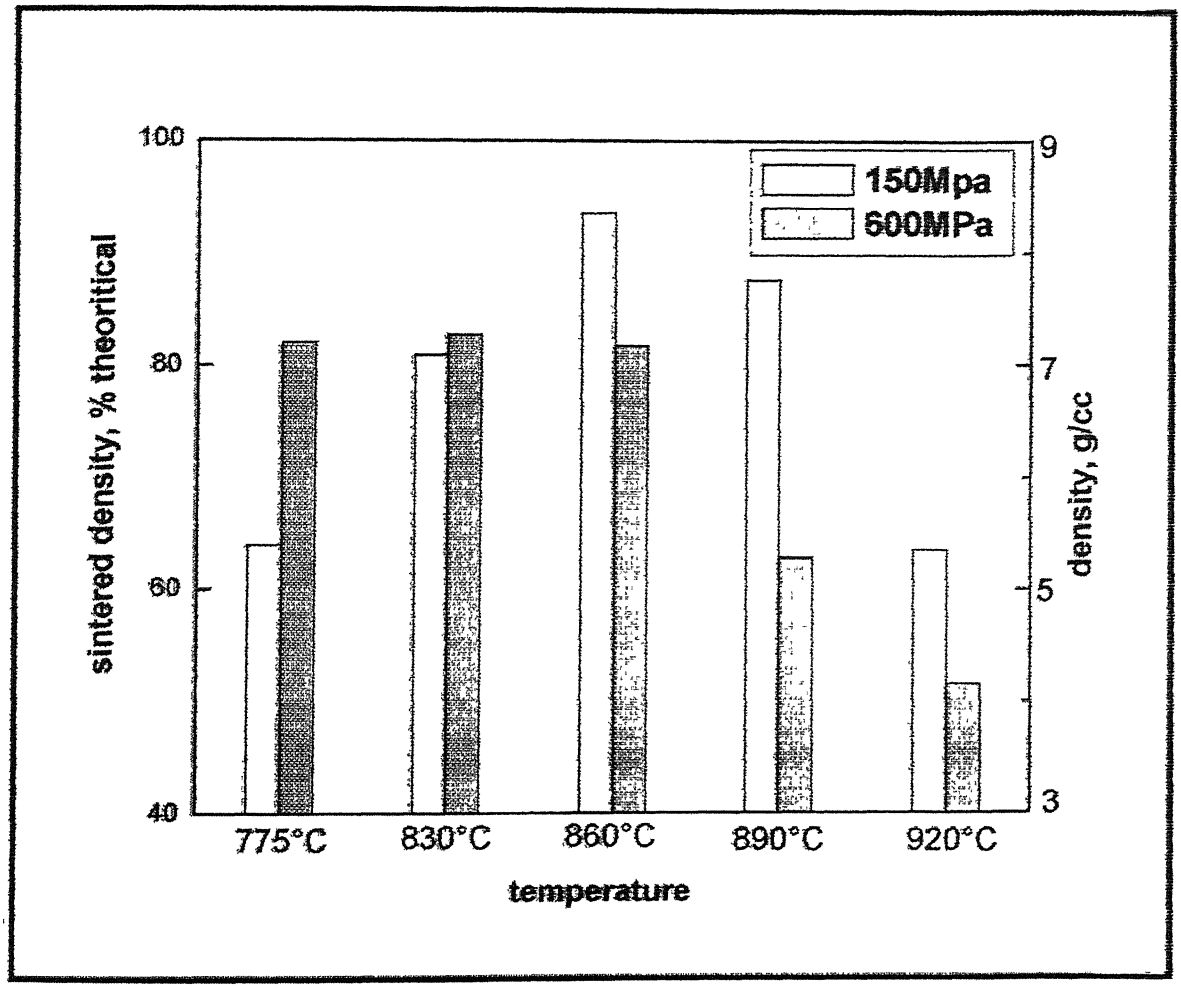

Figure 5.4 Effect of compaction pressure and sintering temperature on the sintered density of the samples.

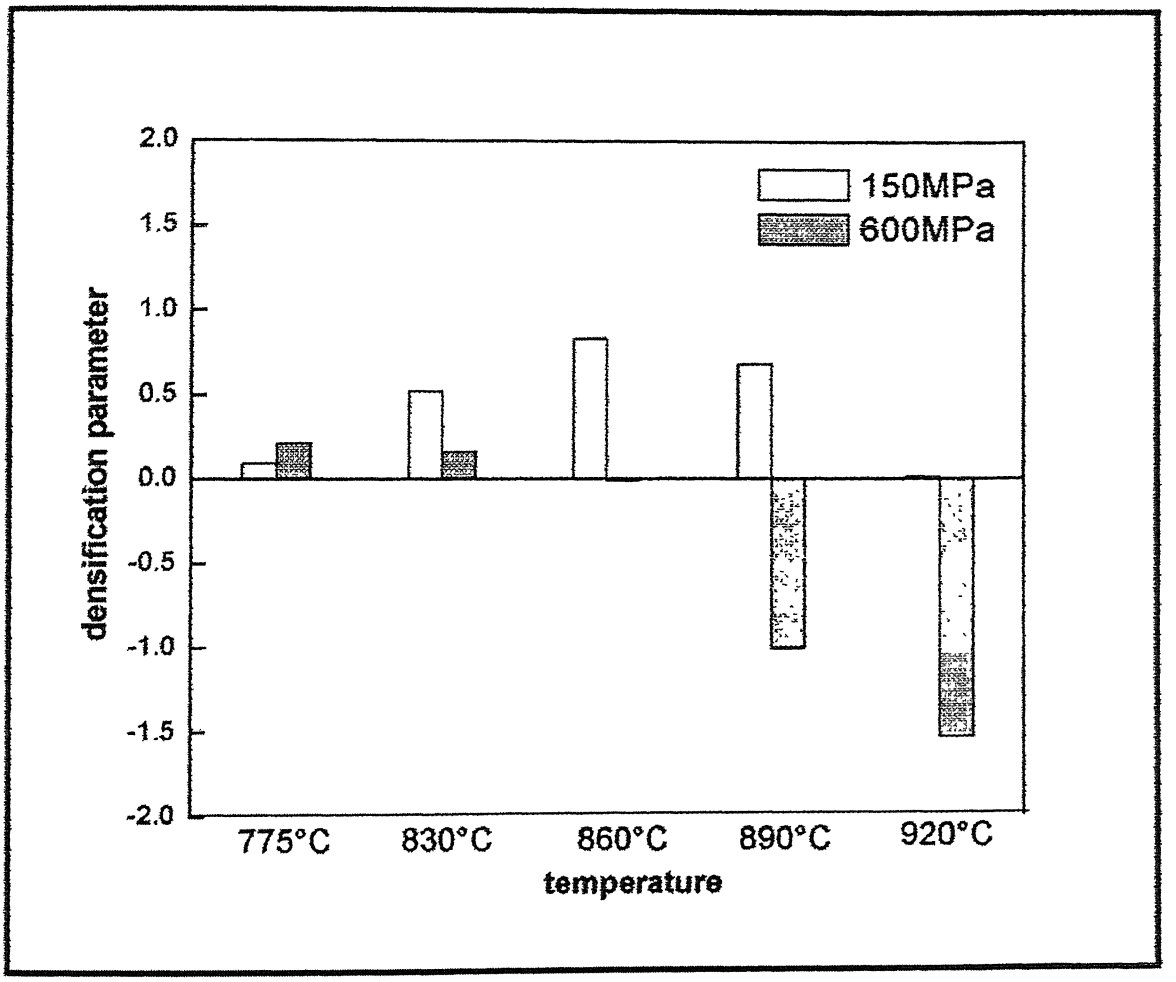

Figure 5.5 Effect of compaction pressure and sintering temperature on the densification parameter.

5.2 Porosity Determination

The porosity of the samples is determined by the xylene impregnation test as described in the Chapter four The experimental results of that experiment are given in the Appendix III The trend in the porosities determined by xylene impregnation test is matching with their value predicted from density determinations which are shown in Appendix II. Figure 5.6 compares the porosity of the samples pressed and sintered at different pressures and temperatures

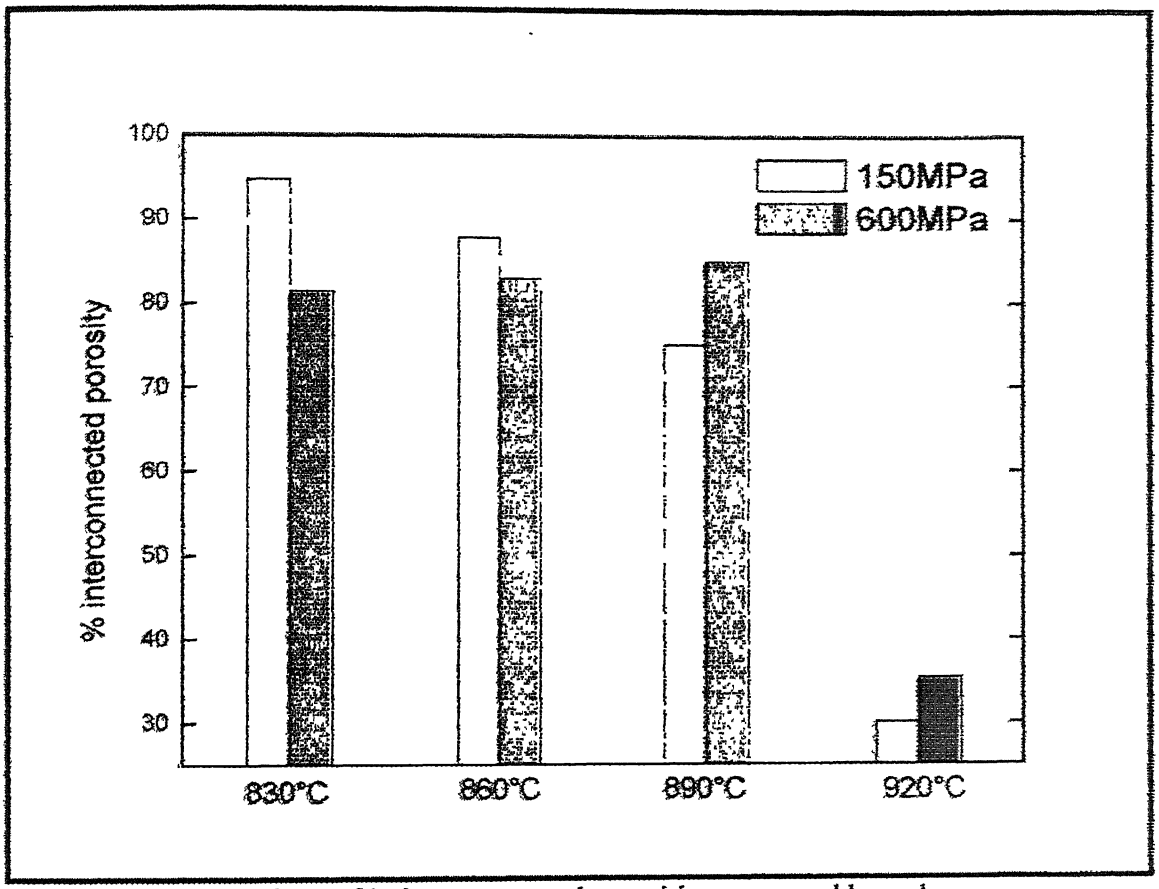

Figure 5.6 Comparison of % interconnected porosities measured by xylene impregnation of both 150 and 600 MPa samples

5.3 Axial and Radial Shrinkage

Appendix IV represents the axial and radial shrinkage data for the samples after sintering Careful observations of the Figure 5.7 shows that 150 MPa samples has undergone shrinkage whereas 600 MPa samples show a differnet approch. There is shrinkage at 830°C but as temperature increases it starts to show expansion At 860°C, there is almos nil expansion/contraction for the 600 MPa sample but with increasing temperature to 890°C, it shows expansion in both radial and axial directions.

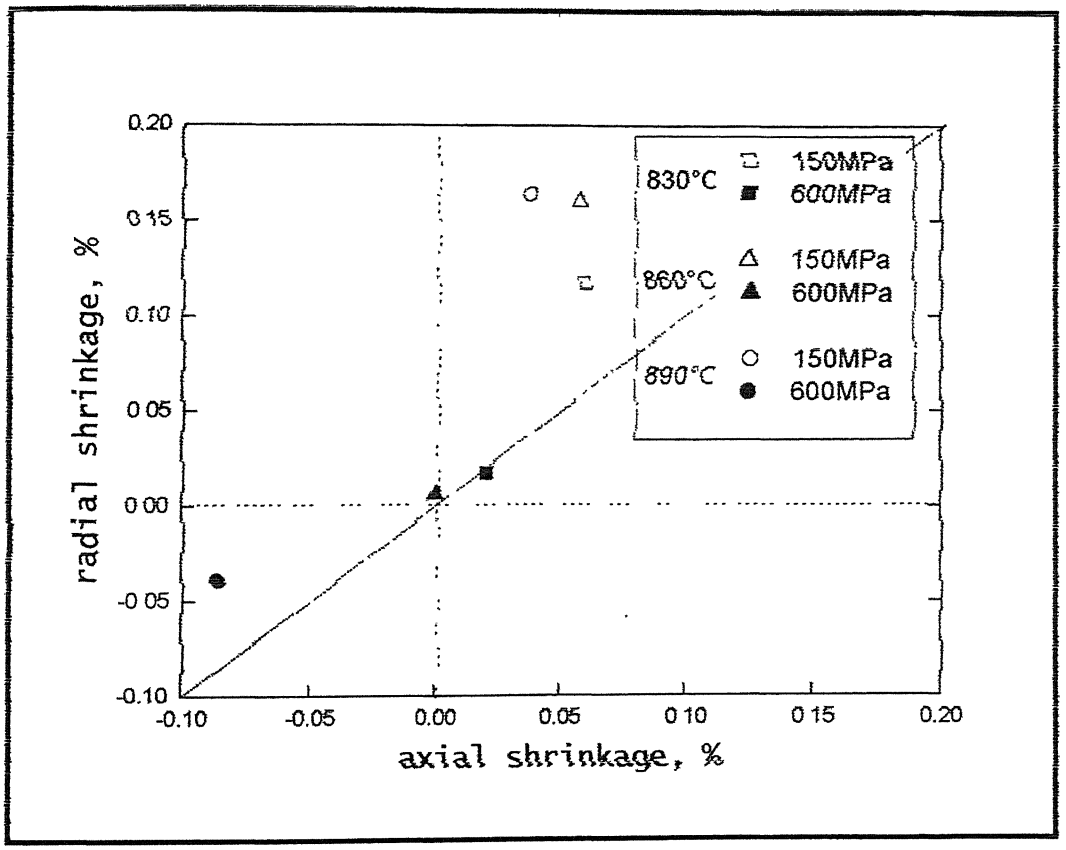

Figure 5.7 Comparison of axial vs. radial Shrinkage at different temperatures for both 150 and 600 MPa samples.

5.4 Macrographs

Figures 5 8 to 5 11 show the macrographs of the samples sintered at different temperatures. Figures 5.8 (a) to 5 11(a) show the macrographs of the as sintered samples whereas Figures 5.8 (b) to 5 11 (b) show the cross-sectional view of the same From the figures it is quite evident, samples sintered at 830 and 860°C do not show any distortion but samples sintered at higher temperatures (i.e. 890 and 920°C) show a significant distortion.

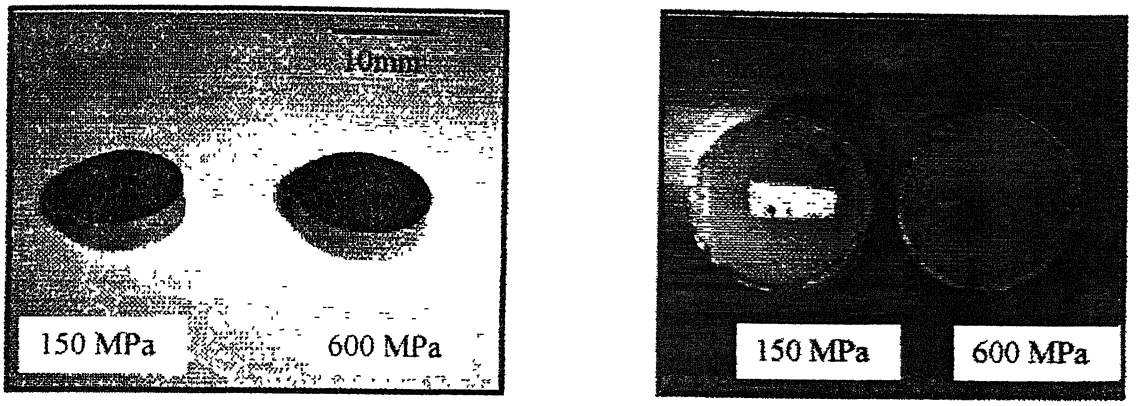

(a) (b)

Figure 5.8 Macrographs of the samples sintered at 830°C.

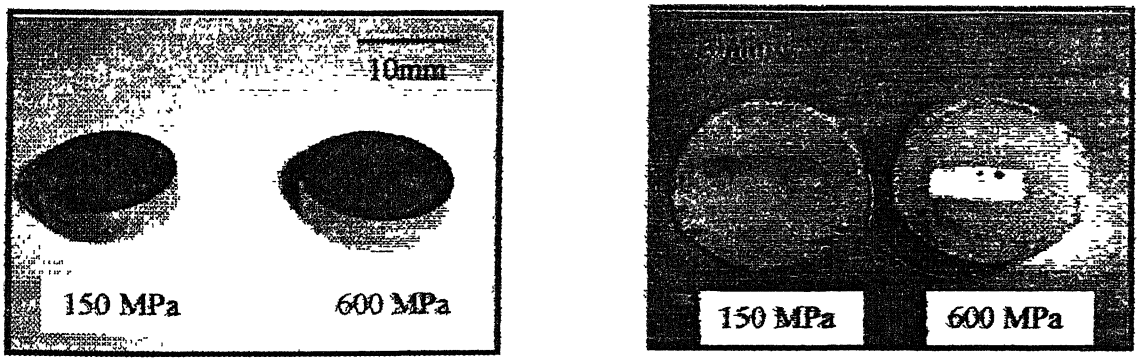

(a) (b)

Figure 5.9 Macrographs of the samples sintered at 860°C.

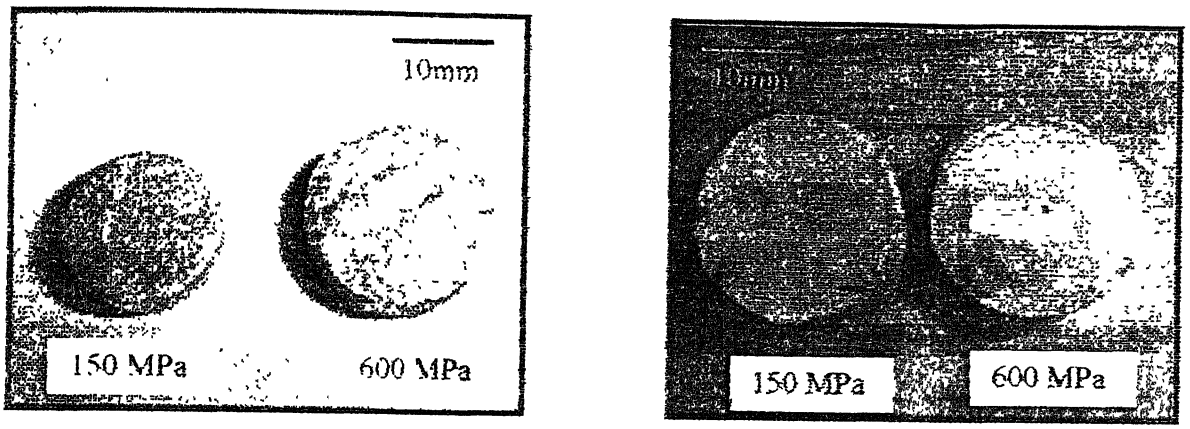

(a) (b)

Figure 5.10 Macrographs of the samples sintered at 890°C.

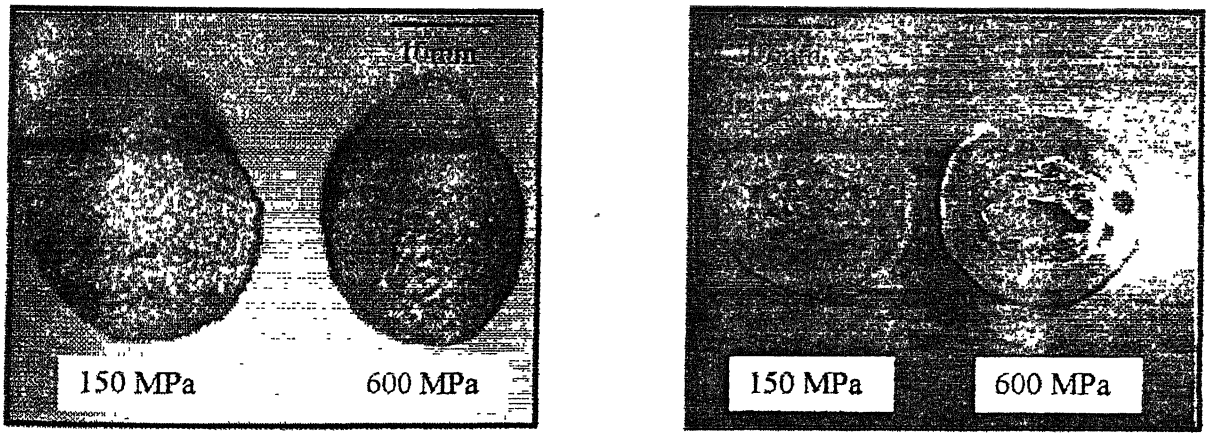

(a) (b)

Figure 5.11 Macrographs of the samples sintered at 920°C.

5.5 Optical Microstructure

Figures 5.12 to 5.29 show the optical micrographs of the sintered samples. From these figures it has been pretty clear that higher the temperature higher is the grain size for 150 MPa samples. However, it is not so in the case of 600MPa samples. 600 MPa samples show higher amount of porosity in the microstructure which can be predicted from their sintered density. The distribution of pores is homogeneous but irregular and size is small in 150 MPa samples whereas in case of 600 MPa samples they are just reversed. The size of the liquid droplet is dependant on the sintering temperature With increasing temperature, higher amount of liquid as well as bigger droplets can be seen in the microstructure.

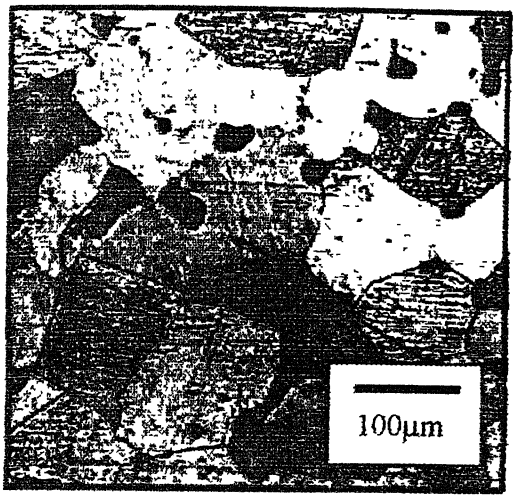

(a)

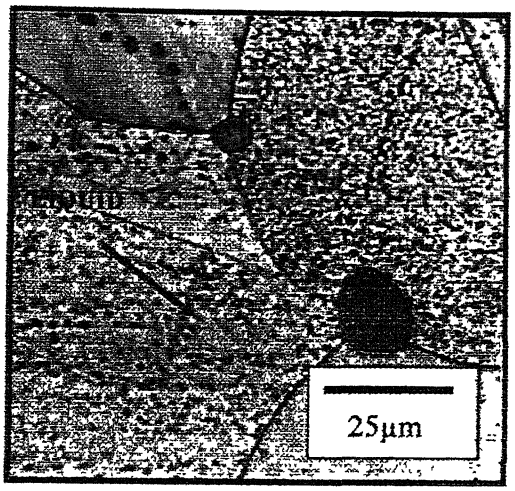

(b)

Figure 5.12 Microstructure of Cu-12%Sn prealloyed compact pressed at 150 MPa and sintered at 830°C.

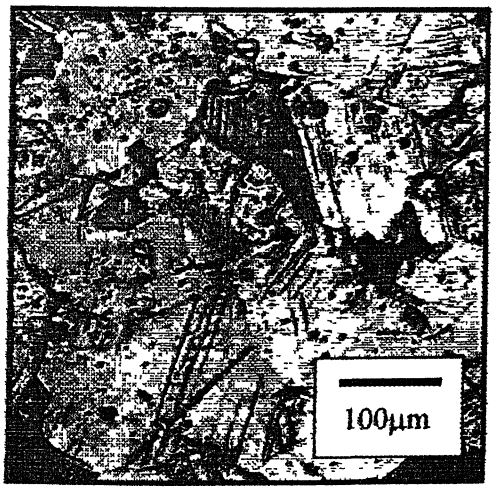

(a)

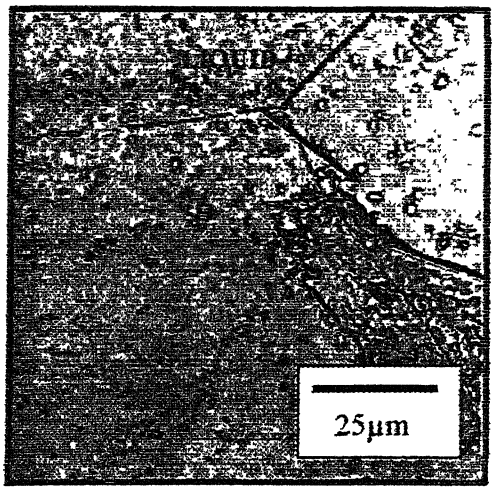

(b)

Figure 5.13 Microstructure of Cu-12%Sn prealloyed compact pressed at 600 MPa and sintered at 830°C

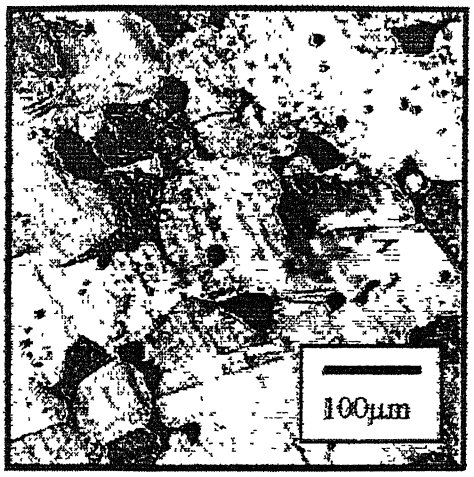

(a)

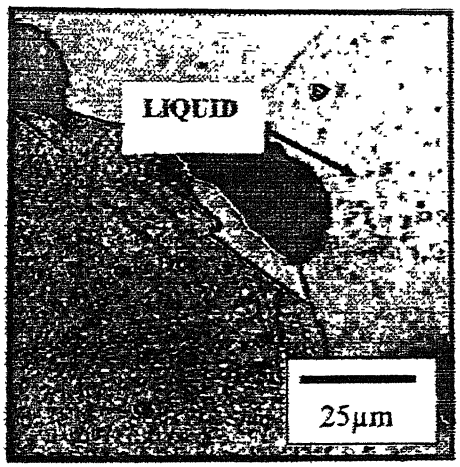

(b)

Figure 5.14 Microstructure of Cu-12%Sn prealloyed compact pressed at 150 MPa and sintered at 860°C.

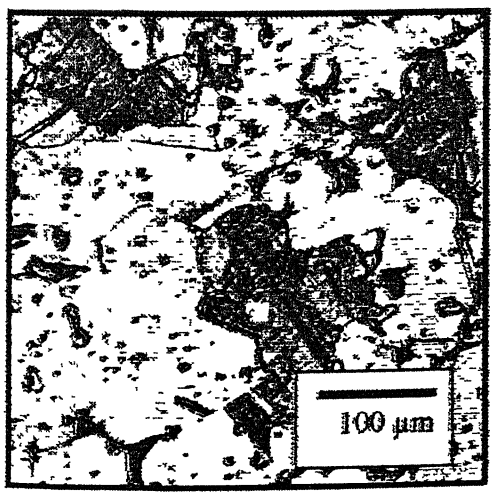

(a)

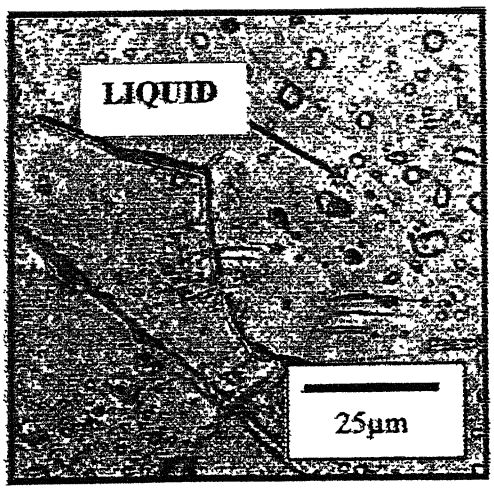

(b)

Figure 5.15 Microstructure of Cu-12%Sn prealloyed compact pressed at 600 MPa and sintered at 860°C.

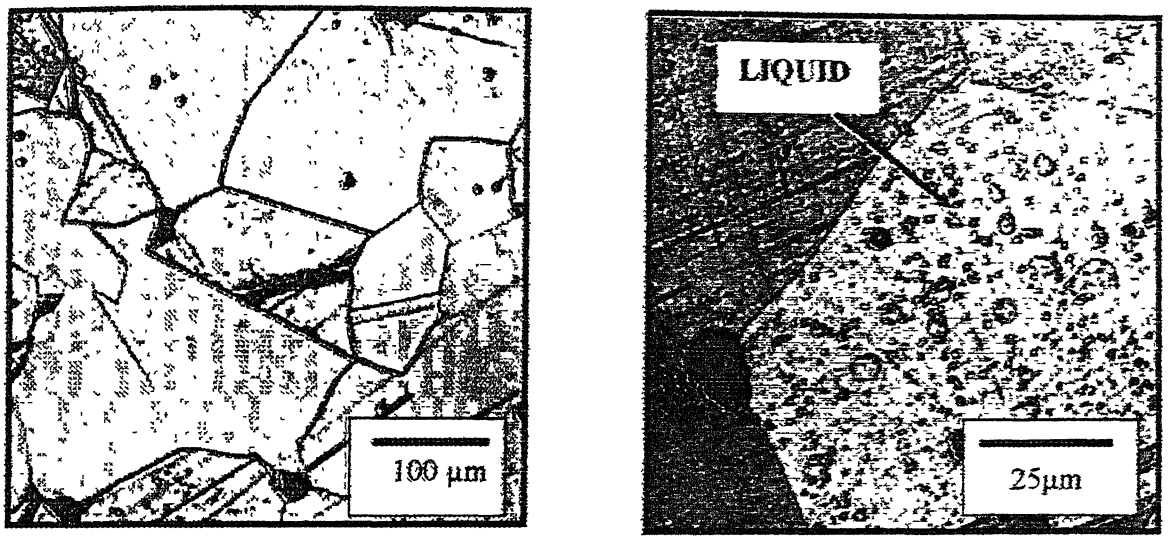

(a) (b)

Figure 5.16 Microstructure of Cu-12%Sn prealloyed compact pressed at 150 MPa and sintered at 890°C.

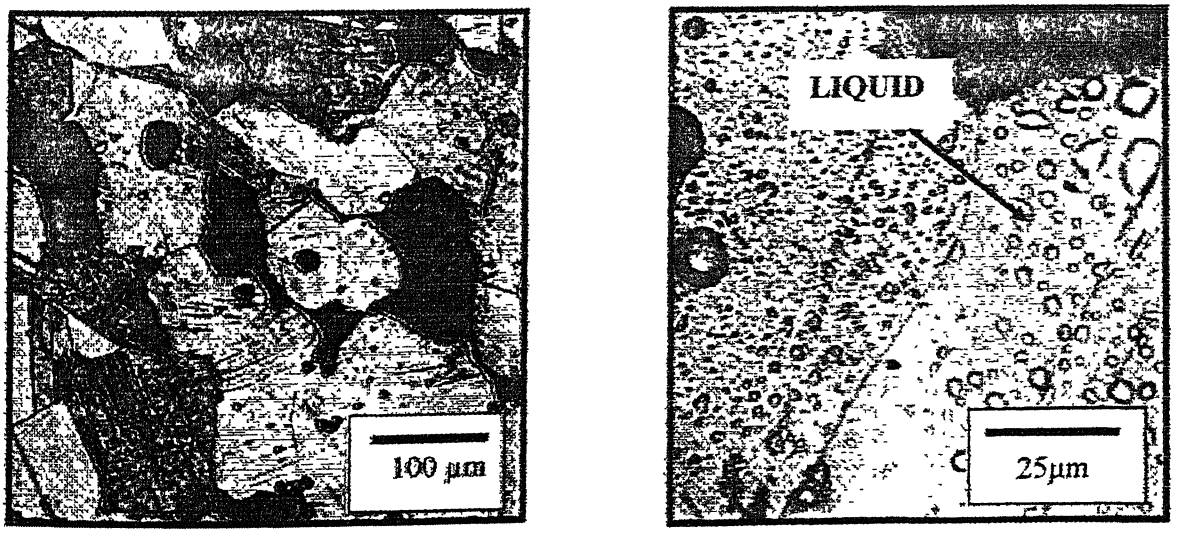

(a) (b)

Figure 5.17 Microstructure of Cu-12%Sn prealloyed compact pressed at 600 MPa and sintered at 890°C.

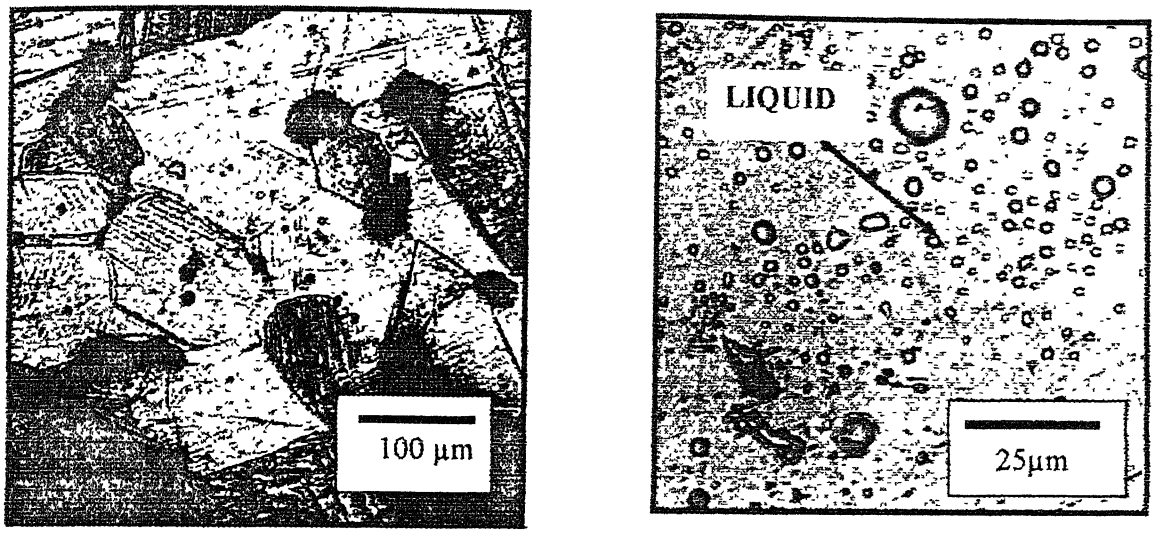

(a) (b)

Figure 5.18 Microstructure of Cu-12%Sn prealloyed compact pressed at 150 MPa and sintered at 920°C.

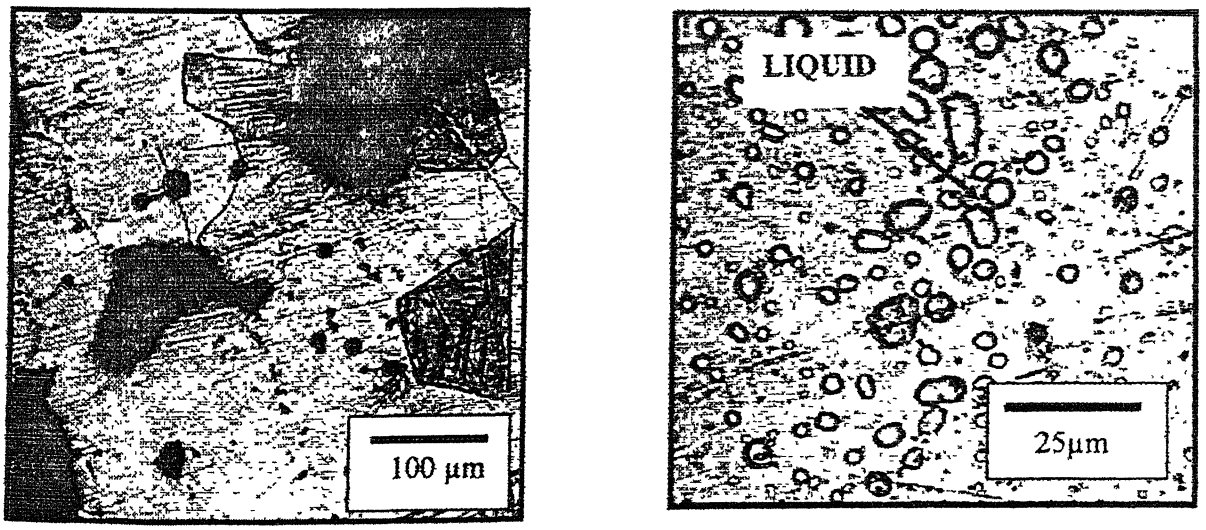

(a) (b)

Figure 5.19 Microstructure of Cu-12%Sn prealloyed compact pressed at 600 MPa and sintered at 920°C

5.6 Hardness Test

5.6.1 Macrohardness

The hardness values obtained from the experimens are given in the Appendix V Hardness data with respect to different temperature and sintered density have been plotted in Figures 5 20 and 5 21, respectively. Comparing 150 and 600 MPa samples, we can conclude that, at higher temperature, i.e.; above 830°C, 150 MPa samples give higher hardness than those of 600 MPa samples. Figure 5.20 clearly indicates that 600 MPa samples, in general, give higher deviation in the hardness values. In case of 920°C, both 150 and 600 MPa samples show highest deviation from the average hardness values. From the Figure 5.21 and the table in the Appendix V, it is obvious that with increasing sintered density, macrohardness values also increase.

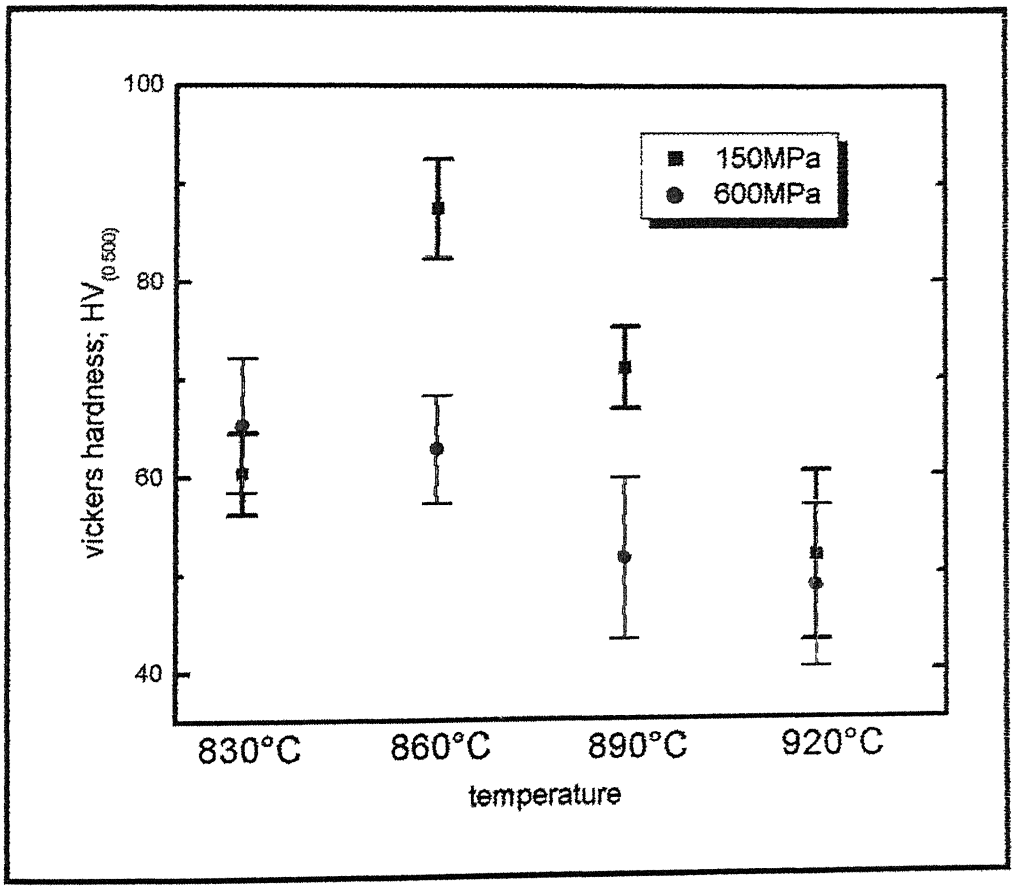

Figure 5.20 Effect of compaction pressure and sintering temperature on the macrohardness of the samples.

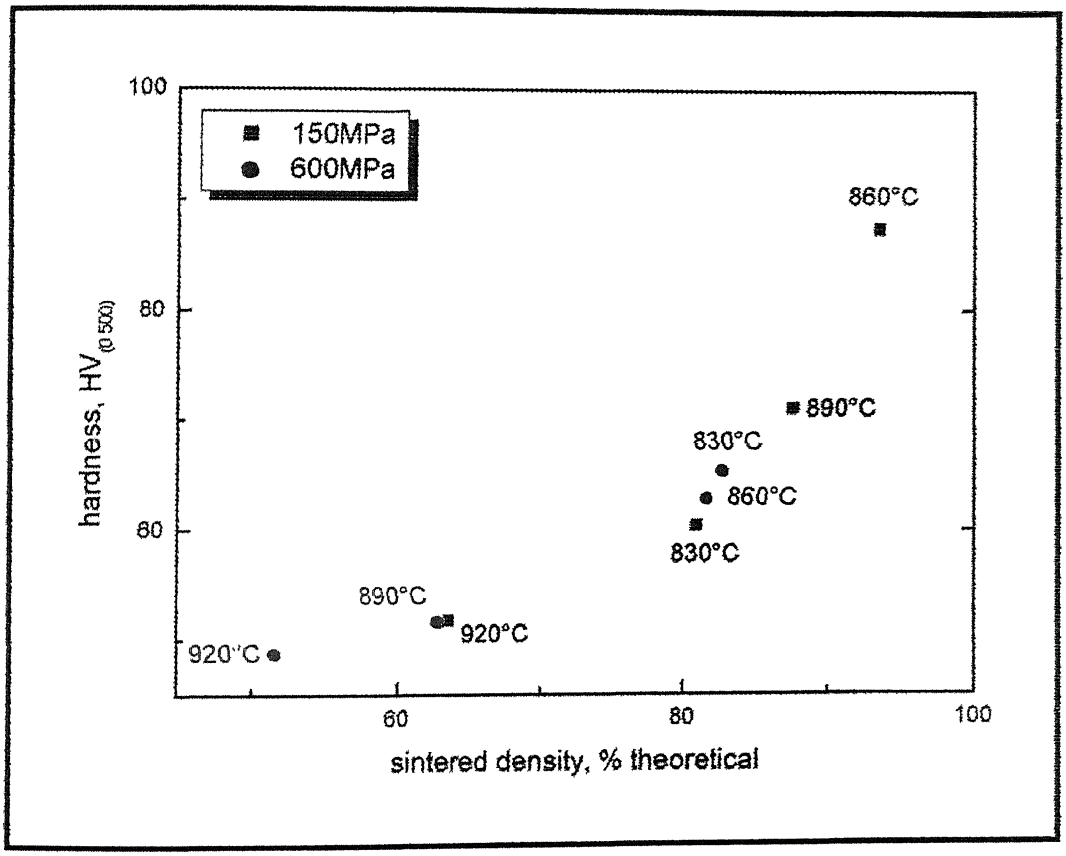

Figure 5.21 Effcet of sintered density on the macrohardness of the sintered compacts.

5.6.2 Microhardness

The microhardness of all the sintered compacts are tabulated in Appendic VI. Effcet of compaction pressure on the microhardness of the compacts are also plotted in Figure 5.22. They are showing that there is a great deal of difference from the macrohardness values. Here, with increasing temperature. hardness of the samples also incraeses, irrespective of the compaction pressure. At the same time, 150 MPa samples always show higher hardness than that of 600 MPa samples at all sintering temperatures and we also got highest hardness for the sample pressed at 150 MPa and sintered at 860°C.

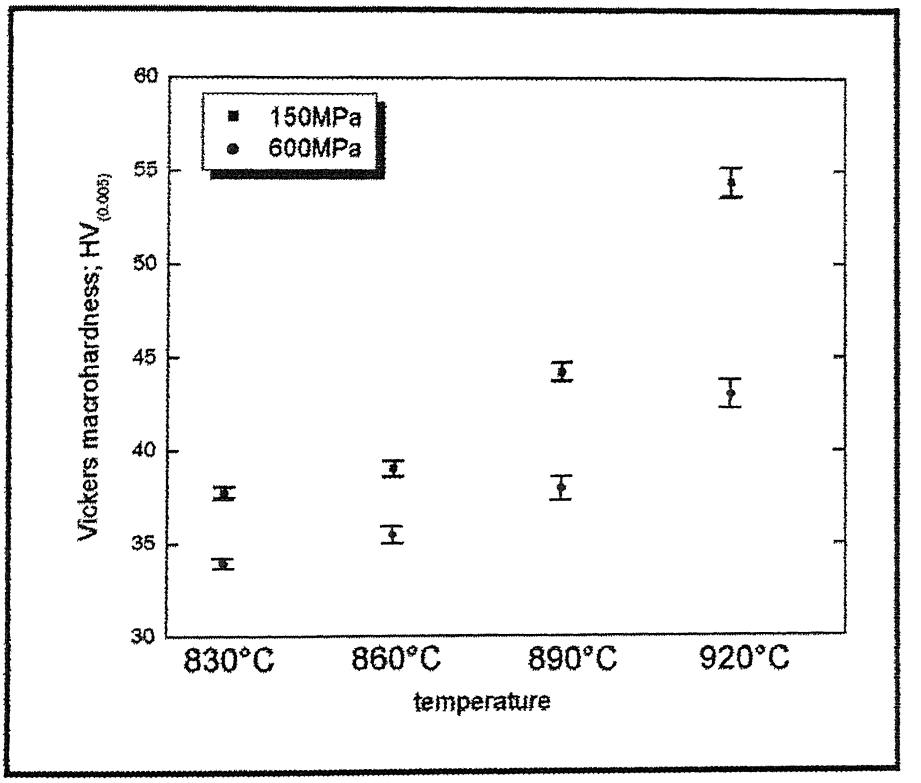

Figure 5.22 Effect of compaction pressure and sintering temperature on micro-hardness.

5.7 X-Ray Diffraction Analysis

XRD diffraction measurements were made to determine if any phase change occur in the sintering compacts which could impact the mechanical properties Figures 5 23 and 5 24 indicate the XRD studies of prealloyed samples (green and sintered) compacted at 150 MPa and 600 MPa, respectively. The prealloyed powder shows α-bronze peak with some intermetallics in green condition. The intermetallic phase is identified as β-$Cu_{5.6}Sn$ from the JCPDS standard chart. XRD study of the powder compact doesn't reveal any tin peak. At the liquid phase sintering condition, there is no trace of the intermetallic phase in the compacts In the final structure only α-bronze is present.

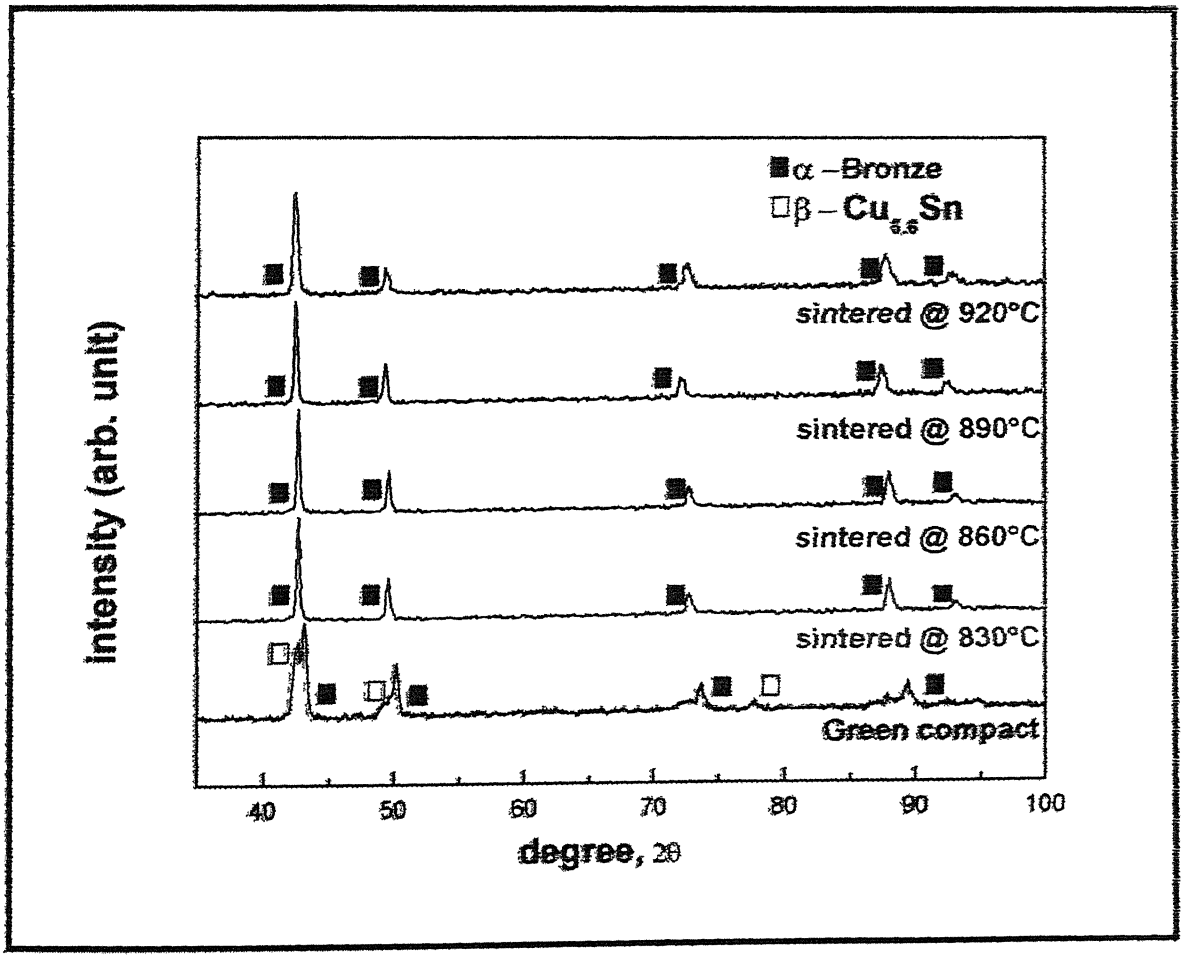

Figure 5.23 X-ray diffraction analyses of 150 MPa samples, as green and sintered conditions

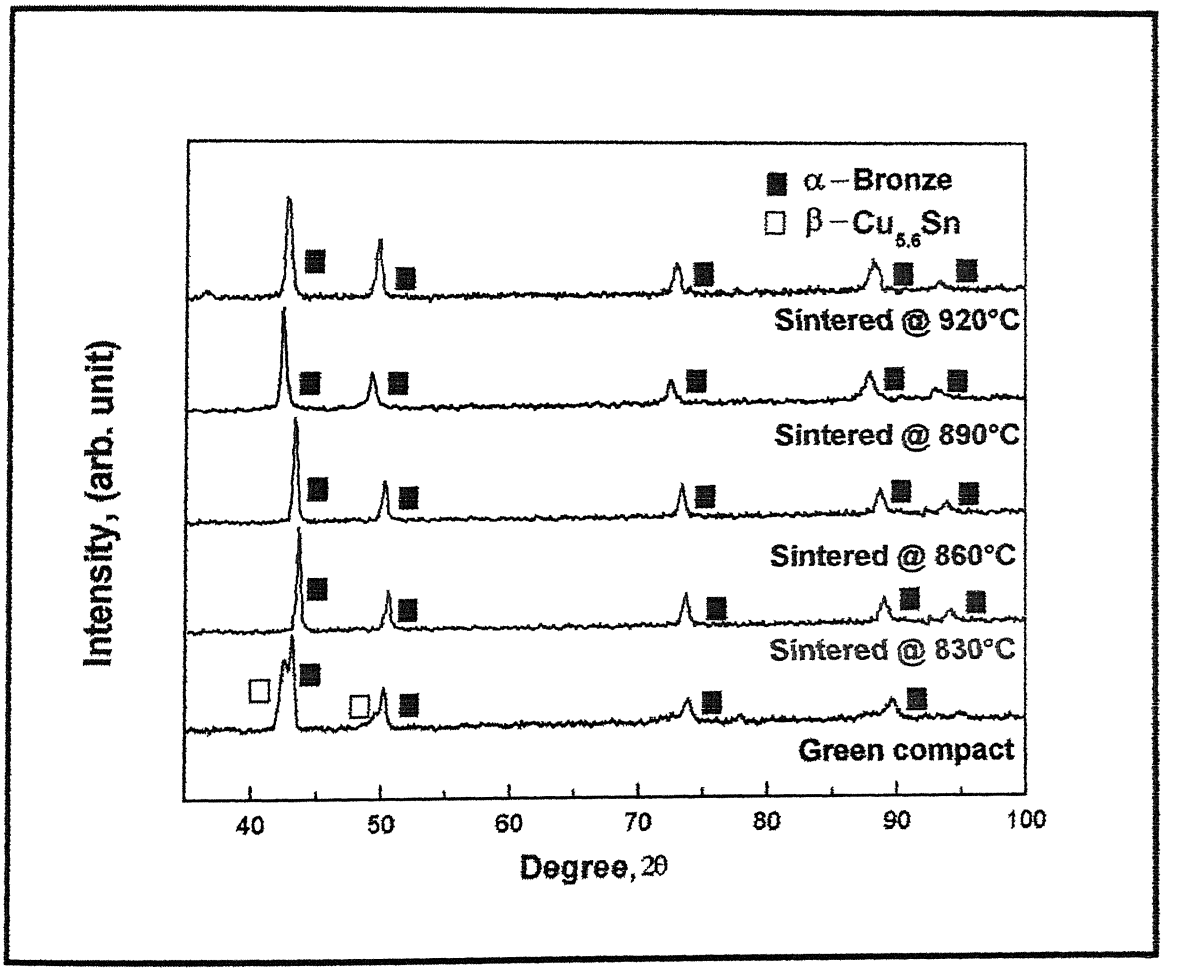

Figure 5.24 X-ray diffraction analyses of 600 MPa samples, as green and sintered conditions.

Chapter 6...

DISCUSSION

DISCUSSION

The results obtained in the present investigation are discussed in this chapter. This chapter is divided into five sections The first section summarizes the changes in density and densification parameters of the prealloyed sintered compacts as a function of sintering temperature along with final porosity. Section two discusses about the radial and axial shrinkage aspect of the sintered samples. Microstructural features are discussed in section three. The very next section discusses the effect of different sintering conditions on the hardness of the samples. Phase evolution on sintering by XRD methods of the samples are discussed in detail in the last section.

6.1 Variation of Sintered Density with Sintering Temperature

As described in the Chapter 4, five different temperatures were selected for the sintering of the prealloyed powder The choice of the temperatures depended on the composition of the alloy. For the present investigation Cu-12Sn composition was chosen and reasons for that have already been mentioned in the section 3.1. From phase diagram of Cu-Sn, it is evident that the solidus and liquidus temperatures for this particular composition are 820°C and 1000°C respectively. According to the phase diagram, 830 to 920°C are in the range between solidus and liquidus temperature, and these temperatures satisfied the supersolidus liquid phase sintering conditions [51]. On the other hand, the temperature of 775°C would correspond to solid state sintering. At any temperature of sintering, the liquid fraction can also be measured from phase diagram. Liquid volume fractions calculated from the phase diagram are given in Table 6.1. The present work compared the effect of different sintering conditions of prealloyed compacts on their various aspects. Effects of

Table 6.1 Volume fraction of liquid formed at different sintering temperature

Sintering Temperature (°C)	Volume Fraction of Liquid (%)
775	0
830	3
860	8
890	27
920	44

pressure on the sintered density variations were also considered.

It has been found that the green density of the compacts increased with increasing pressure as expected Increasing pressure from 150 MPa to 600 MPa brought a change in theoretical density from 60% to 80%. It has been shown in Figure 5.1 that sintered density of the samples pressed at 150 MPa pressure increased with changing sintering condition from solid state (775°C) to supersolidus liquid phase sintering (830°C). This phenomenon can be explained from diffusional kinetic point of view that diffusion of atoms is faster in liquid phase than that in the solid state Increasing sintering temperature increases the sinter density. It attains the maximum value at 860°C temperature. Beyond this temperature, sintered density started to decrease and swelling of compacts took place. This is evident from the Figures 5.8 to 5.11. It may be inferred that during liquid phase sintering the liquid accelerates mass transport and improves sintering densification owing to the capillary forces. In the first step of SLPS, liquid is nucleated at heterogeneous sites, typically at grain boundaries. The liquid spreads on the grain boundaries and attack the solid state interparticle sintered bonds, causing a disintegration of the particles. In turn the wetting liquid provides the capillary force on the structure. The capillary force coupled with the low stress of the wetted grain boundaries allowed rapid repacking and densification. The capillary force is a function of liquid volume fraction. At low sintering temperatures not all boundaries are wet; as a small quantity of liquid forms, consequently there is insufficient fluidity to give complete densification. In this case final densification depends on diffusion through the liquid (termed solution reprecipitation). However, an excess of liquid results in compact slumping, non uniform densification, pore coalescence, and swelling Initially, there were three

phases present, namely solid, liquid, and gas. As the liquid started forming, it went to the pore channels present in the compact by the action of capillary force. If the volume fraction of the liquid is such that it occupied all the pores the system becomes a binary i e solid and liquid. In this condition no capillary force is present A slight increase of liquid from this stage will lead to compact slumping. These problems usually arise when the liquid quantity exceeds 40 vol% [19,31,76].

Thus, there is an optimal temperature range above the solidus temperature that gives a high sintered density, low degree of microstructural coarsening, and minimal compact slumping as shown in Figure 6.1 [19]. In the present study, the optimal temperature has been found to be 860°C for samples pressed at 150 MPa.

In case of samples pressed at 600 MPa, the trend is slightly different. The enhancement of sintered density was not that much from solid state to liquid phase sintering condition as compared to samples pressed at 150 MPa, as shown in Figure 6.2. In compacts pressed at 600 MPa pressure, particle-particle contacts were much higher, and this resulted in high solid state diffusivity. On the other hand, high green density adversely affected the capillary flow of the liquid and hindered the final densification during liquid phase condition [19].

Densification during supersolidus liquid phase sintering (SLPS) is analogous to viscous flow sintering. The prealloyed particles turn mushy and flow once sufficient liquid forms along the grain boundaries [19,26,31,44,53]. The viscosity of a solid-liquid mixture decreases as the liquid volume fraction increases, so more liquid makes for faster sintering but also for less dimensional precision. Compared to solid-state sintering, the densification process shows extreme temperature sensitivity.

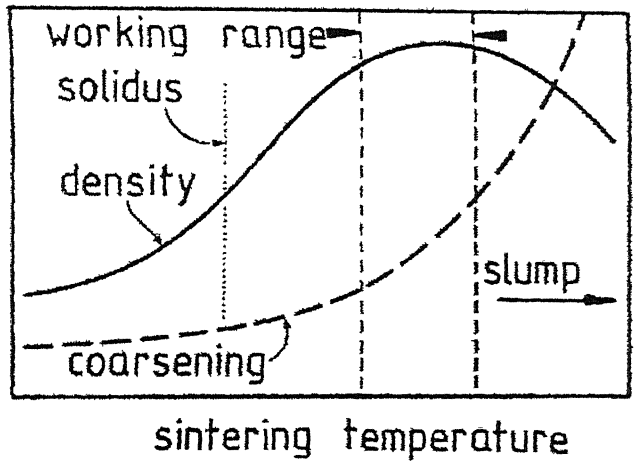

Figure 6.1 A generalized plot of density and microstructural coarsening shown as functions of the sintering temperature [19].

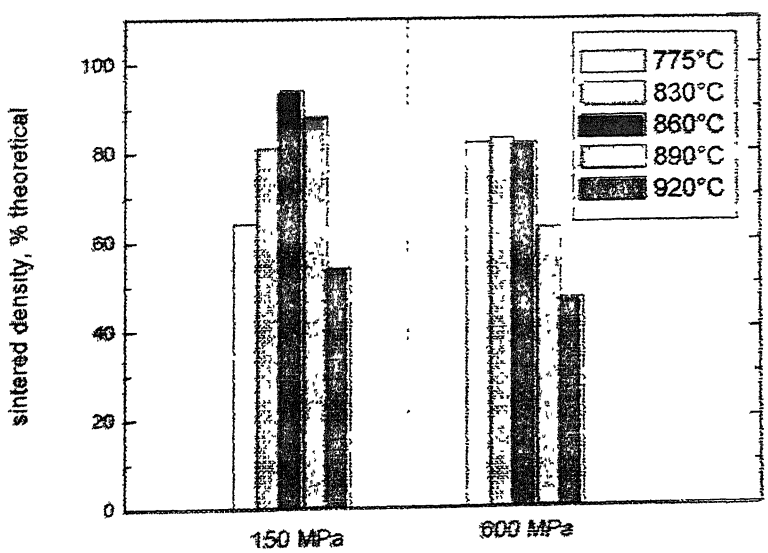

Figure 6.2 Variation in sintered density with temperatures at two different compaction pressures.

Liquid is nucleated at the heterogeneous sites, typically at grain boundaries or interdendritic spaces, where the last solidification took place in powder fabrication The liquid spreads on the grain boundary, causing particle disintegration. As soon as the liquid forms, there is a densification enhancement due to the capillary force exerted by the liquid on the solid particles. Rapidly the solid grains pack to a higher density, releasing liquid to fill pores between grains. It is possible to achieve near full density by rearrangement. During rearrangement the compact exhibits viscous response to the capillary action. The elimination of porosity increases the compact viscosity. As a consequence the densification rate decreases continuously. However, the rearrangement is inhibited by particle contacts form during compaction [53]. In case of 600 MPa samples, particle contacts are more than that of 150 MPa samples and thus rearrangement is poorer which result in lower sintered density for 600 MPa samples. The viscosity of solid liquid mixture decreases as the liquid volume fraction increases, so more liquid makes for faster sintering but also for less dimensional precision. So these two processes counteract each other. At 830°C, the amount of liquid was too small to contribute towards faster sintering. In case of 890 and 920°C, less dimensional precision becomes more dominant and thus swelling and expansion took place. Whereas, in case of 860°C sample, the contribution of liquid towards sintering rate is predominant than that of distortion due to presence of liquid and this is the reason why we have got maximum densification for the sample sintered at temperature 860°C. Again we have got better properties for 150 MPa samples than those of 600 MPa samples. Due to higher compaction pressure, the contact area is higher which contribute to rapid grain coarsening during heating to the sintering temperature for the latter. As a result the liquid which formed at the inter-granular

region is less homogeneously distributed than 150MPa samples which results in less dimensional precision of the samples thus reflected by the densification parameter.

Porosities after sintering were measured by the xylene impregnation test as described in chapter Four. Porosities are removed in the final stage for solid-state sintering. In that stage the isolated, spherical pores are removed by a bulk diffusion mechanism whereas pores located at the grain boundaries are removed more rapidly (almost 100 times) through grain boundary diffusion mechanism. As shown in Figure 5.6, the fraction of interconnected porosity decreased with increasing temperature for both the pressure conditions. In general, with decrease in total porosity results decrease in the fraction of interconnected porosity provided there is no compact distortion takes place. Thus sample sintered at 830°C has higher fraction of interconnected porosity than that of 860°C sample, both pressed at 150 MPa pressures, as the former possessed higher amount of porosity. With further increment in temperature, fractions of the interconnected porosity get lowered down though the total porosity was higher. At that time, the small pores coalesce to form isolated bigger pores. Accordingly, the number of pores decreased and the mean size increased with time, thus resulting in decrement in the fraction of interconnected porosity. The trend remained same for the samples pressed at 600 MPa as well. This fact is clearly revealed from Figure 5.11b.

6.2Variation in Axial and Radial Shrinkage

Careful observation of Figure 5.7 representating the axial and radial shrinkage data for the samples after sintering show that samples pressed at 150 MPa pressure had undergone shrinkage whereas samples pressed at 600 MPa pressure show a differnet approach for samples pressed at 600 MPa pressure, there was shrinkage at

830°C but with increasing temperature it started to show expansion. At 860°C, there was almost nil expansion/contraction but with further increment of temperature to 890°C, it showed expansion in both radial and axial directions. This is because, in LPS, densification and distortion are sequential events, and densification occurs first. Only after near full densification will gravity induced distortion takes place [75]. Thus the sample pressed at 600 MPa pressure and sintered at 860°C, these two forces just balanced each other resulting in almost zero expansion/contraction. With increasing temperature, the latter one became dominant one and ultimately resulted in compact expansion. At the temperature of 920°C, this force became so dominant over densification that compact slumping occurred for both the pressure conditions

6.3 Optical Microscopy

As described in the earlier chapter 5.5 with the help of optical micrographs of the sintered samples (Figures 5.12 to 5.19), there is a great deal of difference in the microstructures of the samples pressed at 150 MPa and 600 MPa. Generally, with increasing temperature grain size of samples should increase due to higher diffusion. Bigger grains eat away the smaller ones, increasing their own area and reducing total number of grains and thus area of grain boundary This phenomenon has been observed in case of samples pressed at 150 MPa. However, samples pressed at 600 MPa pressure, which are less densified after sintering and attained considerably lower sintered density, show a higher amount of porosity in the microstructures. Diffusivity of atom is many fold faster through the metal than that through air. Pores acted as a diffusion barrier to the atoms as they had to pass the pore void to move from one grain to another grain Thus due to presence of higher amount of porosty, grain growth phenomenon had been restricted in 600 MPa samples. The optical micrographs also

show that the distribution of pores were more homogeneous in samples pressed at 150 Mpa than that at the higher pressure (600 MPa) samples This is also the reason why these 600 MPa samples give poorer property, such as less sintered density and hardness. The fact lies in the poorer rearrangement stage during sintering. As the green density increasesd, there was more mechanical interlocking and less pore phase. Consequently, the liquid could not flow into the surrounding pores and the capillary force responsible for rearrangement was reduced.That is in general, densification rate is reduced by a higher green density [53]. With increasing temperature, the amount of liquid in the microstructure also increased, this resulted in liquid droplet qualescence to form bigger droplets in the microstructures for both the pressure conditions.

6.4 Macrohardness

From a comparison of the hardness values for samples pressed at 150 and 600 MPa pressures, it can be concluded that, at higher temperature, i.e.; above 830°C, samples pressed at 150 MPa give higher hardness than those of 600 MPa pressure as they had higher sintered density. As it is clearly indicated in Figure 5.20, samples pressed at 600 MPa pressure, in general, give higher deviation in the hardness values, due to less homoganeity in the microstructure of those samples. In case of sintering at 920°C, both 150 and 600 MPa samples show highest deviation from the average hardness values. At that temperature compacts slumping occurred and much bigger pores formed and also they coalescese to form larger voids inside the samples, thus giving the highest variation in the hardness values obtained by experiment.

6.5 Microhardness

As shown in Figure 5.22, with increasing temperature, hardness of the samples also increased, irrespective of the compaction pressure. At the same time, samples

pressed at 150 MPa have showed higher hardness than the 600 MPa samples at all sintering temperatures. To explain this phenomenon, the basic mechanism of solidification is to be understood. During the time of cooling from liquid stage, the last liquid which solidifies contain maximum percentage of solute and thus this is the hardest. These hard solidified liquid droplets get distributed throughout the matrix and show an effect as similar to that of second phase hardening. Now higher the amount of liquid formed, higher the second phase hardening. We got highest liquid formation in case of sample sintered at 920°C and thus it gave highest hardness Comparing samples pressed at two different pressures, i.e. 150 and 600 MPa, it can be observed that samples pressed at 600 MPa resulted in less hardness than those pressed at 150 MPa. In case of samples pressed at 600 MPa, due to the higher amount of contacts generated during compaction, there was substantial grain growth during heating to the sintering temperature. The liquid which formed at the grain boundary during SLPS, was less homoganeously distributed than the 150 MPa samples, thus giving less hardness when measured in microscopic range.

6.6 Phase Identification by XRD

Figures 5.23 and 5.24 show that the prealloyed powders also contain some second phase at green condition. The prealloyed powders were water atomized and during non-equilibrium cooling some intermetallic might be formed This is expected since slight segregation of the alloy is quite possible during powder production and cooling. The small amount of two-phase material would form with slight variations in composition as the melt cooled to progressively lower temperatures From the JCPDS file the second phase has been identified as β- $Cu_{56}Sn$. Such composition variation would cause shift in the lattice constant and therefore the diffraction pattern. At the

sintering temperatures, the second phase is absent and it can be said that, homogenization was taking place at higher temperature as a result the intermetallic phase was annealed out. All the results indicated an overwhelming dominance of α-bronze

Chapter 7...

CONCLUSIONS

CONCLUSIONS

On the basis of the work done in this Thesis, the following conclusions can be drawn·

1 Prealloyed sintered bronze gives higher strength than premixed bronze due to solid solution strengthening of the initial powder. So it can be used for structural application

2. Supersolidus sintering for the prealloyed samples lead to the higher densification compared to the solid state sintering of the same The effect is more for lower compaction pressure

3 Samples pressed at different pressure conditions, behave differently Densification parameter is higher for samples pressed at higher compaction pressure (600 MPa) than those pressed at lower compaction pressure (150 MPa) during solid state sintering condition, whereas supersolidus liquid phase condition shows reverse results In this case, samples pressed at lower compaction pressure (150 MPa) show shrinkage up to 890°C. Increase in temperature beyond that leads to expansion Whereas samples pressed at higher compaction pressure (600 MPa) show expansion at much lower temperature.

4. Prealloyed samples compacted at 150 MPa show better sintered property, such as higher sintered density, higher hardness, better homogeneity in the microstructure than samples compacted at 600 MPa pressure.

5. Fraction of interconnected porosity becomes less as sintered density increases provided there is no compact distortion. In case of compact slumping, coalescence of pores occurs, which results in less number of pores, with higher mean diameter, in the microstructure. This ultimately reduces the fraction of interconnected porosity.

REFERENCES

REFERENCES

1. From web: www.swissmetal.com
2. S Ghosh, "Processing of Premixed and Prealloyed Bronze through Transient and Supersolidus Liquid Phase Sintering," M Tech Thesis, IIT Kanpur, Kanpur, India, 2001.
3. V. Singh, Physical Metallurgy, Standard Publishers, New Delhi, India, 1999, pp 664-668.
4. B.T.K. Barry and C J. Thwaites, Tin and Its Alloys and Compounds, Ellis Horwood Ltd., West Sussex, England, 1983.
5. G.S. Upadhyaya, Sintered Metallic and Ceramic Materials.
6. Ivan Nikitich Frantsevith, Poroshkovaya Metallurgia. n. 7/8, 1995, p 2.
7. Industry Statistics, Metal Powder Industries Federation, 1996, p. 873.
8. ASM Handbook, v 7, Materials Park, OH, USA, 1998, pp 864-866.
9. ASM Handbook, v.2, Metals Park, OH, USA, 1990.
10. H M Wiilliams, General Motors Corporation, U.S Patent 1,556658, 1925
11. H.M Wiilliams and A.L.Boegehold, General Motors Corporation, U S. Patents 1,642,347; 1,642,348; and 1,642,349, 1927
12. C. Claus, Bound-Brook Oilless Bearing Company, U.S. Patent 1,607,389, 1926.
13. G. F. Castedo, "A Study of Bronzes with Different Tin Contents by using Computer Assisted Statistical Techniques," *Powder Metallurgy Science and Technology*, v 4, n. 2, 1993, pp. 24-28.
14. H. C. Neubing, "Properties and Sintering Behaviours of Spherical Tin-Bronze Powders for the Manufacture of Filters," *Powder Metallurgy International*, v. 18, n. 4, 1986, pp. 278-285.
15. R. Merhar, "Consolidation of Powders," Copper Base Powder Metallurgy, v. 7, P.W. Taubenblatt (eds) MPIF, 1980.
16. G.S. Upadhyaya, Powder Metallurgy Technology, Cambridge International Science Publishing, Cambridge, England, 1999.
17. R.M. German, Sintering Theory and Practice, John Wiley & Sons, New York, USA, 1998.

18. D.F. Berry, "Factors Affecting the Growth of 90/10 Copper/Tin Mixes Based on Atomized Powders," *Powder Metallurgy*, v. 15, 1972, pp. 247-266

19 R.M German, "Supersolidus Liquid Phase Sintering. Part I. Process Review," *International Journal of Powder Metallurgy*, v. 26, n. 1, 1990, pp. 23-34

20. W. J Huppmann, "Sintering to High Density," *The International Journal of Powder Metallurgy and Powder Technology*, v. 21, 1985, pp. 183-191

21 R Tandon, "Densification Mechanisms and Microstructural Evolution leading to high density Processing of Prealloyed Powders in Supersolidus Liquid Phase Sintering," Ph.D. Thesis, The Pennsylvania State University, University Park, PA, USA, 1995.

22. L. Cambal and J. Lund, "Supersolidus Sintering of Loose Steel Powders," *International Journal of Powder Metallurgy*, v. 8, 1972, pp. 131-140

23. J. Lund, R.G. Butters, and C.H. Weaver, "Supersolidus Sintering of Prealloyed Monel Powders," *Powder Metallurgy International*, v. 4, 1972, pp. 173-174.

24. G. D. Lawrence, and G. S. Foster, "Pressureless Sintering of Aluminium Powder," *Metals Engineering Quarterly*, v. 11, 1971, pp. 25-30.

25. E. J. Westerman, "Sinteriong of Nickel based Superalloys," *Transactions of the Metallurgical Society of AIMI*, v. 224, 1962, pp. 159-164.

26. J Lund, and S. R. Bala, "Supersolidus Sintering," Modern Developments in Powder Metallurgy, H. H. Hausner, and W E. Smith (eds.), MPIF, Princeton, NJ, v. 6, 1974, pp. 412-421.

27. S.R. Bala, J. Lund, "Studies of the Supersolidus Sintering of Cupro-nickel Powder," *Zeitschrift fuer Metallkunde*, Bd. 70, 1979, pp. 185-190.

28. C. Guyard, C. H. Allibert, J. Driole, and G. Raisson, "Liquid Phase Sintering of Prealloyed Powders of Co-based alloys," *Science of Sintering*, v 13, 1981. pp. 149-163.

29. S. Takajo, and M. Nitta, "Observation of Liquid Phase Sintering of a High Speed Steel Powder," Sintering'85, G. C. Kuczynski, D. P. Uskovic, H. Plamour, and M. M. Ristic (eds.), 1987, Plenum Press, NY, pp. 189-196.

30. P. Murley, and R. M. German, "Supersolidus Sintering of Coarse Powders and its Application to Powder Injection Molding," *Advances in Powder Metallurgy*, v. 3, MPIF/APMI, Princeton, NJ, 1989, pp. 103-120.

31 R M. German, "Supersolidus Liquid Phase Sintering. Part II. Densification Theory," *International Journal of Powder Metallurgy*, v. 26, n 1, 1990, pp. 35-43.

32 R M German, "A Quantitative Theory for Supersolidus Liquid Phase Sintering," *Powder Metallurgy*, v. 34, 1981, pp. 101-107

33 C. S. Wright *et. al*, "Densification of T1-High Speed Steel Powder by Vacuum Sintering," *Powder Metallurgy*, v. 32, 1989, pp. 109-113.

34. M. Santos *et. al.*, "Optimisation of Processing Parameters for Direct Vacuum Sintering of T15-High Speed Steel," *Powder Metallurgy*, v. 34, 1991, pp. 93-100.

35. C. Toennes, and R.M. German, "Density and Microstructure Control in Martensitic Stainless Steel through Enhanced Sintering," *Powder Metallurgy International*, v. 24, 1992, pp. 151-157.

36. B.P. Saha, and G. S. Upadhyaya, "Liquid Phase Sintering of T15 and T42 High Speed Steel Composites Containing Ti(C,N)," *Powder Metallurgy International*, v. 24, 1992, pp. 345-350.

37. R. H. Palma and *et. al.*, "Sintering Behaviour of T42 Water Atomised High Speed Steel Powder under Vacuum and Industrial Atmospheres with Free Carbon Addition," *Powder Metallurgy*, v. 32, 1989, pp. 291-299.

38. P. K. Kar, and G. S. Upadhyaya, "Liquid Phase Sintering of P/M High Speed Steels," *Powder Metallurgy International*, v. 22, 1990, pp. 23-26.

39. S. Jauregi and *et. al.*, Influence of Atmosphere on Sintering of T-15 and M-2 Steels Powders," *Metallurgical Transactions* A, v. 23A, 1992, pp. 389-400.

40. P.Maulik, and W.J.C. Price, "Effect of Carbon Addition on Sintering Characteristics and Microstructure of BT42 High Speed Steel," *Powder Metallurgy*, v.30, 1987, pp. 240-248.

41. R. Tandon, Y. Liu, and R.M. German, "Application of Supersolidus Liquid Phase Sintering to High Density Processing of Prealloyed Powders," *Advances in Powder Metallurgy and Particulate Materials*, 1995.

42. P.J. Wray, "The Geometry of Two Phase Aggregates in which the Shape of the Second Phase is Determined by its Dihedral Angle," *Acta Metallurgy*, v. 25, 1976, pp. 125-127.

43 H.H. Yoon, and D.N. Yoon, "Effect of Dihedral Angle on the Morphology of Grains in a Matrix Phase," *Metallurgical Transaction A*, v.16A, 1985, pp 923-926.

44. R. Tandon, and R.M. German, "Particle Fragmentation during Supersolidus Sintering," *The International Journal of Powder Metallurgy*, v 33, n 1, 1997, pp. 54-60.

45. R. Tandon, and R.M. German, "Supersolidus Transient Liquid Phase Sintering using Superalloy Powders," *International Journal of Powder Metallurgy*, v. 30, 1994, pp. 435-443.

46. R. Tandon, Y. Liu, and R.M. German, "High Density Processing of Ferrous Alloys via Supersolidus Liquid Phase Sintering," Advances in Powder Metallurgy and Particulate Materials, 1995.

47. W. A. Kaysser, and G. Petzow, "Present State of Liquid Phase Sintering," *Powder Metallurgy*, v. 28, 1985, pp. 145-150.

48. W.J. Huppmann, "The Elementary Mechanism of Liquid Phase Sintering; II: - Solution Reprecipitation," *Z. Metallkunde*, Bd. 70, H. 11, 1979, pp. 707-713.

49. R.M. German, Powder Metallurgy of Iron and Steel, John Wiley Publishing, NY, USA, 1998.

50. A. Lal, "Mechanisms and Mechanics of Shape Loss During Supersolidus Liquid Phase Sintering," Ph.D. Thesis, The Pennsylvania State University, University Park, PA, USA, 1999.

51. R. Tandon, and R. M. German, "Sintered and Mechanical Properties Of A Boron Doped Austenitic Steel," *International Journal of Powder Metallurgy*, v. 34, n. 1, 1998, pp 40-49.

52. R.M. German, "Dimensional Changes in Mixed Powder Sintering," Advances in Powder Metallurgy and Particulate Materials-1995, Metal Powder Industries Federation, Princeton, NJ, 1995, pp. 4.113-4.126.

53. R.M. German, Liquid Phase Sintering, Plenum Press, New York, NY, 1985, pp. 1-155.

54 G Dowson, "The Sintering of Bronze," *Metal Powder report*, 1984, n. 2, pp. 71-73.

55 B. Krishnakant and M. Patel, "Superior Quality Bronze Bearings," Modern Developments in Powder Metallurgy, v 19, P.U. Gummeson and D.A. Gustafson (eds.), MPIF, Princeton, NJ, USA, 1988, pp. 621-640.

56. M. M. Collur, and G. S. Upadhyaya, "Sintering of 9% Tin-Bronze with Iron Addition through Premixed and Prealloyed Routes," *Transactions PMAI*, v 9, 1982, pp. 35-40.

57 H.E Hall, "Sintering of Copper and Tin Powders," *Metals and Alloys*, 1939, pp 297-299.

58. D.F. Berry, "Factors Affecting the Growth of 90/10 Copper/Tin Mixes Based on Atomized Powders," *Powder Metallurgy*, v. 15, 1972, pp. 247-266.

59. E. Deegan and A.D. Sarkar, "Effect of Sintering Variables on the Dimensional Changes of Copper-Tin Compacts up to 10% Tin," *Metallurgia and Metal Forming*, v. 40, n. 8, 1973, pp. 148-151.

60. A.B. backensto, "Changes in Dimensional Change for Bronze Premixes as Premix Components Changes," Modern Developments in Powder Metallurgy, v.19, P.U. Gummeson and D.A. Gustafson (eds.), MPIF, Princeton, NJ, USA, 1988, pp. 641-652.

61. D.F. Berry, E. Klar and N. Veloff, "Aspects of Dimensional Control During Manufacture of Bronze Self Lubricating Bearings," Advances in Powder Metallurgy and Particulate Materials, v. 6 , 1992 , Metal Powder Industries Federation, Princeton, NJ, USA, pp. 51-61.

62. R. Davis and A.D. Sarkar, "Volume Growth of Copper-Tin Compacts due to Sintering with Tin Content Between 12–20%," *Metallurgia and Metal Forming*, v.40, n.8, 1973, pp. 260-261.

63. E. Peissker, "Pressing and Sintering Characteristics of Powder Mixtures for Sintered Bronze 90/10 Containing Different Amounts of Free Tin," Modern Developments in Powder Metallurgy, v. 7, H.H. Hausner and W.E. Smith (eds.), 1974, pp. 597-614.

64. N.N. Acharya, P.G. Mukunda, and A. Bose, "Properties of Vacuum Sintered Bronze Bearings – Influence of Copper Powder," *Powder Metallurgy International*, v. 16, n. 5, 1984, pp. 212-216.

65. J.W. Kim, S.J. Kang, D.N. Yoon, "The Flow Behaviour of Sn Melt During Sintering of 90Cu-10Sn Powder Compacts, *Powder Metallurgy International*, v 19, n 3, 1987, pp 41-42.

66. K Das and J A. Bas, "Control of Delta Phase in 90/10 Bronze Bearings," Advances in Powder Metallurgy and Particulate Materials, v. 6, 1992, Metal Powder Industries Federation, Princeton, NJ, USA, pp. 23-34.

67. N N. Acharya and P.G Mukunda, "Sintering in the Copper-Tin System, Part I: Identification of Phases and Reactions," *The International Journal of Powder Metallurgy*, v. 31, n 1, 1995, pp. 63-71.

68. N N. Acharya and P.G. Mukunda, "Sintering in the Copper-Tin System, Part II: Alloy Behaviour," *The International Journal of Powder Metallurgy*, v. 31, n. 1, 1995, pp. 73-79.

69. N.N. Acharya and P.G. Mukunda, "Sintering in the Copper-Tin System, Part III: Influences of Variables," *The International Journal of Powder Metallurgy*, v. 31, n. 1, 1995, pp. 81-88.

70. J.I. Farmer, "Microstructure of Non-Ferrous PM Materials," *Metal Powder Report*, v 38, n. 5, 1983, pp. 256-260.

71. N.N Acharya and P G Mukunda, "Metallography of Copper-Tin Alloys," *Metallography*, v. 21, 1988, pp. 137-150.

72. C. Messner and *et. al*, "Effect of Copper Powder on the Liquid Phase Sintering of 10% Tin-Bronze," Proceedings of 2000 Powder Metallurgy World Congress, pp 701-704.

73. C. Menapace and *et. al*, "Radial Crushing Strength of Tin-Bronze Bearings Produced with Different Copper Powders: Effect of Density and Pore Morphology," *Powder Metallurgy Progress*, v. 2, n. 1, 2002, pp. 19-31.

74. G. Arthur, "Porosity and Permeability Changes During the Sintering of Copper Powder," *Journal of the Institute of Metals*, v. 83, 1954-55, pp. 329-336.

75. Wumen *et. al.*, "Linking Microstructure and Macrostructure during LPS under Gravity", MPR, July/August, 2000.

76. J.Liu, A.L.Cardamore, and R.M.German, "Estimation of Capillary Pressure in Liquid Phase Sintering", *Powder Metallurgy*, v. 44, n. 4, 2001, pp. 317-324.

APPENDICES

Appendix I

Experimental data for the green samples

Sintering Temperature (°C)	Compaction Pressure (MPa)	Height (cm)	Diameter (cm)	Weight (g)	Volume (cm^3)	Density (g/ cm^3)	% theoretical density
775	150	0.620	1.277	4.158	0.79	5.30	61.03
775	600	0.531	1.277	4.539	0.67	6.76	78.38
830	150	0.530	1.277	3.537	0.67	5.27	60.51
830	600	0.571	1.277	4.997	0.72	6.92	79.49
860	150	0.401	1.277	2.770	0.51	5.40	61.89
860	600	0.341	1.277	3.115	0.44	7.15	81.96
890	150	0.431	1.277	2.952	0.55	5.36	61.42
890	600	0.413	1.277	3.756	0.53	7.11	81.53
920	150	0.433	1.277	2.866	0.55	5.18	59.37
920	600	0.396	1.277	3.579	0.51	7.06	80.97

Appendix II

Experimental data after sintering

Sintering Temperature (°C)	Compaction Pressure (MPa)	Height (cm)	Diameter (cm)	Weight (g)	Volume (cm^3)	Density (g/cm^3)	% theoretical density	Weight loss %	Densification Parameter
775	150	0.600	1.25	4.11	0.74	5.59	64	1.06	0.09
775	600	0.510	1.25	4.49	0.63	7.18	82	1.06	0.21
830	150	0.47	1.16	3.5	0.50	7.05	80.94	1.03	0.52
830	600	0.55	1.26	4.94	0.69	7.21	82.78	1.10	0.16
860	150	0.34	1.12	2.74	0.34	8.15	93.48	1.08	0.83
860	600	0.34	1.27	3.08	0.43	7.13	81.72	1.09	-0.014
890	150	0.39	1.11	2.92	0.38	7.64	87.61	1.08	0.68
890	600	0.50	1.32	3.72	0.68	5.48	62.83	1.08	-1.012
920	150	Distorted		2.85	0.61	4.67	53.57	0.44	-0.143
920	600	Distorted		3.55	0.87	4.08	46.74	0.77	-1.798

Appendix III

Experimental data for xylene impregnation test

Compaction Pressure (MPa)	Sintering Temperature (°C)	Wt before impregnation A1 (gm)	Wt after impregnation		Porosity	
			In air B (gm)	In water C (gm)	Total (%)	% Interconnected
150	830	3.4222	3.5964	2.9765	34.0	94.7
600	830	4.9384	5.1024	4.3029	29 0	81.4
150	860	2.6691	2.7051	2.3519	13.3	87.9
600	860	3 0795	3.1688	2.6924	25.9	83 0
150	890	2 8680	2.9294	2.5065	22.2	75.1
600	890	3.709	3.8970	3.2177	37.4	85.0
150	920	2 8497	2.9192	2.3273	44.8	30.1
600	920	3.5500	3.6810	2.8495	51.0	35.3

Appendix IV

Axial and radial dimensions of the samples

Condition	Before Sintering		After Sintering		Axial Shrinkage %	Radial Shrinkage %
	Ht. (mm)	Dia. (mm)	Ht. (mm)	Dia (mm)		
150 MPa, 830°C	5 3	12.77	4.7	11.6	0.06	0.117
600 MPa, 830°C	5 7	12 77	5.5	12.6	0.02	0 017
150 MPa, 860°C	4 01	12 77	3 43	11 17	0.058	0.016
600 MPa, 860°C	3 41	12 77	3.41	12.71	0.0	0 006
150 MPa, 890°C	4 31	12.77	3.93	11.13	0.038	0.164
600 MPa, 890°C	4.13	12.77	4.99	13.16	-0.086	-0.039

\+ shrinkage

\- expansion

Appendix V

Hardness values of the samples

Sample	No of Observation	D1	D2	Hardness $HV_{0\,500}$	Average hardness HV	Deviation
150 MPa, 830°C	1	99 1	101	55.6	60 4	4.17
	2	98.7	97.2	58		
	3	95.3	96.3	60.3		
	4	95.4	95.1	61.4		
	5	90.8	91.8	66.7		
600 MPa, 830°C	1	90 5	94 4	65.1	65.48	6 90
	2	101.2	102.4	53.7		
	3	118.3	112.7	69.6		
	4	88.4	89.1	70.6		
	5	119 3	113 5	68.4		
150 MPa, 860°C	1	100.5	87.5	87.5	87.44	5.11
	2	106.3	110.9	78.6		
	3	100 1	102.5	90.3		
	4	100.0	101.9	91.0		
	5	98.9	104.3	89.8		
600 MPa, 860°C	1	125.0	134.4	55.1	62.98	5.51
	2	118.1	115.8	67.8		
	3	121.0	126.8	60.4		
	4	119.3	113.5	68.4		
	5	92.8	94.8	63.2		

150 MPa, 890°C	1	119.9	120 8	64.0	71.14	4.22
	2	112 0	113 5	72 9		
	3	109 8	112.5	75.0		
	4	115.0	113 2	71 2		
	5	115.0	111.0	72 6		
600 MPa, 890°C	1	127.5	135.0	53.8	51.74	8.31
	2	118.9	119.9	65.0		
	3	109 1	115.2	44 2		
	4	103.3	107.6	50		
	5	108.5	112 1	45.7		
150 MPa, 920°C	1	149.5	147 9	41.9	51.80	8.69
	2	127.2	115 3	63.1		
	3	141.0	138.9	47.3		
	4	117.6	134.3	58.4		
	5	107 9	106.9	48.3		
600 MPa, 920°C	1	146.9	137.5	45.8	48.82	8.35
	2	132.1	132.2	53.1		
	3	121 8	124.1	61.3		
	4	163.1	131.5	42.7		
	5	115.3	117.1	41.2		

Appendix VI

Microhardness of the sintered compacts

Sample	Compaction Pressure	Sintering Temperature	Hardness HV_{005}					Average hardness
Cu-12%Sn	150MPa	830°C	37.8	38.2	37.5	37.7	37 4	37 72
Cu-12%Sn	600MPa	830°C	33.5	34.2	34.1	33.9	34.1	33.96
Cu-12%Sn	150MPa	860°C	38.6	39 6	44.1	44 1	38 6	41.00
Cu-12%Sn	600MPa	860°C	34.9	35.3	35.3	35.3	35.8	35 32
Cu-12%Sn	150MPa	890°C	44.1	44.7	43.5	44.7	44 1	44.42
Cu-12%Sn	600MPa	890°C	37.6	38.1	38.6	37.1	38.6	38.00
Cu-12%Sn	150MPa	920°C	54.9	54.9	54.9	53.2	54.0	54.38
Cu-12%Sn	600MPa	920°C	44.1	42.9	42.9	42.1	43 5	43.1